Steady State Entanglement in Quantum Dot Networks

Anine Laura Borger

Master's thesis in Physics,
Niels Bohr Institute,
University of Copenhagen

Supervisor	Associate Professor Mark S. Rudner
Co-Supervisors	Professor Karsten Flensberg
	Professor Anders S. Sørensen

Submitted
March 1, 2016

Acknowledgements

First and foremost, I would like to thank Associate Professor Mark S. Rudner who has been my primary supervisor. Thank you for your time, patience, and encouragement. Your guidance has been invaluable for the project and my learning process. I also thank my secondary supervisors Professor Karsten Flensberg and Professor Anders S. Sørensen for support and good ideas on how to proceed.

Apart from my formal advisors, I have had fruitful discussions on my project with a large number of people. Thanks to all of you. I will especially like to bring forward Konrad Wölms, Esben Bork Hansen, Jens Rix, Nina Rasmussen, Mathilde Thorn Ljungdahl, and Cilie Hansen.

A great thanks to Cilie Hansen, Esben Bork Hansen, Samuel Sanchez, Pernille Saugmann, Freja Pedersen, Asbjørn Arvad, Christian Berrig, Bjarke Mønsted, Sofie Janas, Ida Viola Andersen, Christoffer Østfeldt, Nina Rasmuseen, Anders Bakke, Asbjørn "Darling" Drachmann, and Sissel Bay Nielsen for proofreading (parts of) the report. I owe a great thanks on the layout of the document to Esben Mølgaard and Bjarke Mønsted.

A special thanks goes to the lunch club and other passionate colleagues for pleasant breaks during the office days. I thank the group of the knitting physicists, Strikkelogen, for help with the common thread. Thanks to everyone who made it an invaluable experience to be a student at the Niels Bohr Institute and a part of the cabaret, FysikRevy™, to tutor new students in Vildledergruppen, to freeze with the winter swimming club, T_c, discuss politics in the student council, Fagrådet, and simply having a cup of coffee in the student lounge |RUM|.

I would like to thank my parents and my kitchen at Studentergården, Psykopat, for great support and encouragement. Last but not least: Jonas Bundgård Mathiassen, you were there for me throughout this process every time. Thank you.

Contents

List of Figures

Abstract

We propose to engineer the coupling of quantum dot networks to reservoirs such that the steady state of electron transport through the network has a large population of a specific multi-electron entangled state. Specifically, we investigate whether the coupling of a linear triple dot network to reservoirs can be tuned such that the steady state has a large population of the spin singlet state with one electron on each of the outer dots as a proof of concept. We find the steady state population by numerically solving the master equation for the triple dot modeled as an open quantum system. The master equation is derived under the Born and Markov approximations. We then compare the results to a perturbative estimate of the population. Our results show promise for engineering the coupling of the triple dot network to reservoirs such that it has a large steady state population of the desired singlet state. This approach and its generalizations to larger networks may provide new routes for dissipative preparation of multi-particle entanglement in solid state quantum circuits.

CHAPTER 1

PREFACE

Quantum computers are devices which perform computations actively using the quantum mechanical properties of its bits or "qubits". They are highly interesting because they might solve certain types of problems much faster than the computers we know today.[1] One choice for implementing the qubits of such a device is to encode information in the spin of a single electron in a quantum dot.

One of the important experimental requirements for realizing a quantum computer is to create a specific initial state of the qubits which can be manipulated to perform computations.[2] We propose to engineer the coupling of quantum dot networks to source and drain reservoirs such that the steady state of transport through the dot network has a large population in a specific entangled state. This could provide a new way of initializing qubits, which we hope may be generalizable to even more complex spin states.

In the thesis, we work on a simple example as a proof of concept. Our system is a linear triple dot network with smaller outer dots and a bigger middle dot. We assume that the bias window is such that all states of the network with three or more electrons are inaccessible and that only the low energy orbitals of the dots can be occupied. More specifically, we assume that only the two lowest energy orbitals on the middle dot can be occupied and that there cannot be more than one electron on each of the outer dots, which must reside in the corresponding orbital ground state. The outer dots are coupled to source reservoirs and the middle dot is coupled to a drain reservoir. The goal of the project is to investigate whether the coupling of the triple dot network to the reservoirs and its

internal parameters can be tuned such that the steady state of transport through the network has a large population of the singlet state with one electron on each of the outer dots.

The main ingredient for achieving the large singlet population on the outer dots is the exchange splitting between the spin singlet and triplet states occupying two orbitals. We aim at tuning the network parameters and the couplings to the reservoirs such that the desired singlet state on the outer dots is off-resonant with the singlet states on the middle dot and thus blocked in transport through the dot network while the triplet states with one electron on each of the outer dots are resonant with the triplet states on the middle dot and thus not blocked.

We investigate the steady state populations in the dot network using a perturbative approach and also by finding the steady state of the system's master equation derived under the Born and Markov approximations.

In chapter 2, we place the project in its scientific context by introducing quantum computers, the challenges in their experimental realization, quantum dots and known blockade phenomena in transport through quantum dots.

In chapter 3 we derive the master equation of open quantum systems under the Born and Markov approximations and construct a numerical tool to set up the master equation and find its steady state. As a warm-up we apply the master equation and the numerical tool to single and two-level systems, where we can compare the output of the numerical tool with exact, analytical results.

In chapter 4, we set up a Hamiltonian for the triple dot network and estimate the steady state population of the triple dot network using a perturbative approach and find the steady state of the master equation for the network.

In the remaining chapters, we discuss the results of the previous chapter, the model limitations and the numerical implementation, conclude on our work, and present the natural next steps.

We assume that the reader is familiar with quantum mechanics in first and second quantization, but as a reminder we include a brief summary of the concepts used in the thesis in App. A. In the main text, we introduce the key concepts of entanglement and density operators for pure and mixed states.

Chapter 2

Introduction

This chapter serves as a brief introduction to the scientific context of this project. The chapter covers the following topics: Quantum computers and the challenges in their experimental realization as well as quantum dots and known blockade phenomena in transport through quantum dots.

2.1 Quantum Information Processing

Our proposal of preparing specific spin states by engineering the coupling of a quantum dot network to reservoirs could be useful for realizing quantum computers. In this section, we give a brief introduction to quantum computers that covers the quantum circuit model for quantum computation and the requirements to a physical system that should serve as qubits. The first part of the section is based on Ref. [3].

Research in quantum computers is highly interesting because it deepens our understanding of quantum mechanics and they can be used for efficient quantum simulation[4] shine new light on topics as high T_c superconductivity, quantum magnetism, and quantum phase transitions[5]. It has been shown, theoretically, that quantum computers solve certain types of problems much more efficiently than classical computers.[6] A few examples of the early quantum algorithms, which provide a significant speed-up compared to classical algorithms, are Grover's algorithm for search in an unsorted data base and Shor's algorithm for factorization of large numbers. Grover's algorithm provides a quadratic speed-up and Shor's algorithm provides an exponential speed-up.[3]

The quantum mechanical bit, usually refered to as the "qubit", is the smallest chunk of quantum information. It can in principle be stored in the state of any quantum two-level system, which has the properties described in Sec. A.1 on pure states. The state of multiple qubits is in general a superposition. Here we give the general state of two qubits as an example

$$\left|\psi\right\rangle = c_{00}\left|0\right\rangle_1\left|0\right\rangle_2 + c_{01}\left|0\right\rangle_1\left|1\right\rangle_2 + c_{10}\left|1\right\rangle_1\left|0\right\rangle_2 + c_{11}\left|1\right\rangle_1\left|1\right\rangle_2 . \tag{2.1}$$

For N qubits there are 2^N terms in the superposition if none of the coefficients are zero.

Quantum Parallelism, which gives quantum computers an advantages over classical computers, arises from the possibility to prepare the state of qubits in a superposition. This allows us to perform a computation on all the states of the qubits:$|0\rangle_1|0\rangle_2$, $|0\rangle_1|1\rangle_2$, $|1\rangle_1|0\rangle_2$, and $|1\rangle_1|1\rangle_2$ at once. However, we need to come up with a clever algorithm to exploit quantum parallelism, because a read-out of the result of the computation is done by measuring the value of (some of) the qubits and that collapses the qubit state, as described in Sec. A.2 about measurement.

One way to perform quantum computations is the quantum circuit model. In the quantum circuit model, computation is performed by applying a sequence of unitary transformations to qubits initialized to a known state. The result of the computation is obtained by measuring the state of the qubits.[3] To initialize the qubit state means to prepare the system in a known state from which we can perform calculations.[2]

There are five requirements for the physical implementation of quantum computers described by DiVincenzo, and the last part of this section is based on his article Ref. [2]:

1. a scalable physical system with well characterized qubits
2. the ability to initialize the state of the qubits
3. long decoherence times compared to the gate operation time
4. a set of quantum gates with which all calculations can be performed
5. the capability of performing measurements on specific qubits.

The first two requirements are most central to the aim of the thesis. The ability to initialize is covered in the section above, so we elaborate on the scalable physical system with well characterized qubits only. We refer to Ref. [2] for more details on the latter three.

Well characterized qubits means first of all that we need to be able to isolate two levels of the system that can serve as qubit states and secondly that we need to understand the dynamics of the individual qubits and the coupling between qubits such that we may manipulate their state. The system needs to be scalable because we need more than a few qubits for any practical purpose.

2.2 Quantum Dot Based Spin Qubits

One specific choice of qubit implementation is the spin of a single electron confined in a quantum dot[7][8][9]. In this section, we describe quantum dots and electron transport through dots. In the description of transport, we emphasize the Coulomb and Pauli blockade phenomena, because we want to employ a new blockade phenomenon in initializing the triple dot network. We return to this in Chap. 4.

This section is primarily inspired by the article "Spins in few-electron quantum dots" by Hanson et al.[10].

2.2.1 Quantum Dots

A quantum dot is a (pseudo-)zero dimensional system where electrons are confined in all spatial dimensions on a small enough length scale such that the energy spectrum becomes discrete.[10]

Size Requirements of Quantum Dots

In an experimental setup, the energy spectrum of the dot is broadened due to interactions with the environment such as couplings to an electron reservoir[11] or non-zero temperature. However, if the broadening of each level in the spectrum is much smaller than the energy difference between levels, we may still regard the spectrum as discrete.

We make an order of magnitude estimate of the length scale we need to confine electrons on in order to regard the spectrum as discrete. To do this, we model the confining potential of the dot as an infinite well potential. In the infinite well potential, the energy of the nth level is proportional to n^2, and the level spacing between the nth and $(n+1)$th level scales with n. For more details on the infinite well potential, we refer to App. A. So the smallest gap occurs between ψ_1 and ψ_2. We consider thermal broadening only which broadens the levels by $k_B T$. Thus we may consider the spectrum discrete if $\varepsilon_2 - \varepsilon_1 \gg k_B T$.

The experiments reviewed in Ref. [10] are typically conducted in dilution refrigerators with a base temperature of 20 mK. We assume that electrons also have the temperature $T = 20$ mK and the effective mass $m^* = 0.067m$[12] where m is the free electron mass. For these parameters, the width of the well has to fulfill $a \ll \frac{3\hbar^2\pi^2}{2m^*k_BT} \approx 3$ μm in order for the two lowest states in the well to be considered discrete despite thermal broadening. From this estimate, the diameter of the dot should be on the order of a few hundred nanometers. The value is consistent with the experimental setups shown in Fig. 2 b) and c) in Ref. [10] Hanson et al.

Lateral Quantum Dots

There are several ways to realize quantum dots experimentally: Single molecules trapped between between leads, semiconductor nanowires, carbon nanotubes, self-assembled dots and lateral and vertical semiconductor dots.[10] In this thesis, we focus on lateral dots because they have a high degree of tunability.[10]

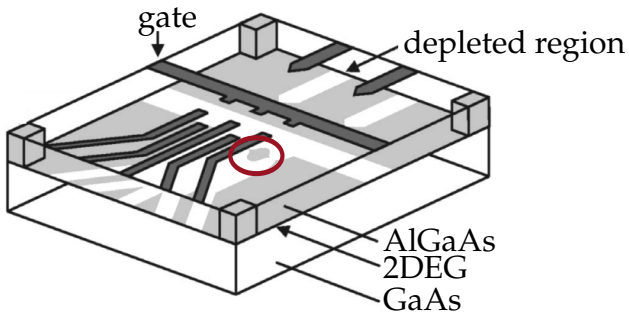

Figure 2.1: Lateral quantum dot device. The block is a heterostructure of doped AlGaAs and GaAs. A 2DEG (light gray) forms at the interface. Charging the gates (dark grey) on top of the block with electrons depletes the 2DEG by forming an electrostatic potential. Quantum dots are isolated areas of the 2DEG. One is encircled in red near the middle of the figure. With the gates we may tune the confining potential and the tunneling coupling. The figure is adapted from Ref. [10] by Hanson et al.

We show a sketch of a lateral quantum dot in Fig. 2.1. The block is a heterostructure with a layer of doped aluminum gallium arsenide (AlGaAs) on top of a gallium arsenide (GaAs) layer. The AlGaAs layer is doped to provide free electrons. The light grey plane illustrates that a two dimensional electron gas (2DEG) of free electrons forms at the interface

where they are confined vertically.[10] On top of the block drawn, we find gates (dark grey). The gates are used to deplete the electron gas locally.

It is done by charging the gates with electrons which repel the electrons in the 2DEG so the electrostatic potential confines the electrons in the plane of the 2DEG. We refer to the potential well at the interface of the heterostructure and the electrostatic potential as the confining potential. Quantum dots are formed as small islands of undepleted 2DEG. Via the gates it is possible to control the potential of each dot and their couplings.[10]

2.2.2 Electron Transport in Quantum Dots

Electron transport through a quantum dot network is a sequence of tunneling events where an electron tunnels from the source reservoir through the dots and to the drain reservoir. We illustrate this in Fig. 2.2 for n dots on a row.

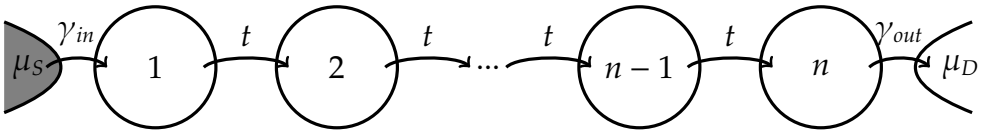

Figure 2.2: Electron transport through a quantum dot network. Electron transport through a quantum dot network is a sequence of tunneling events where an electron tunnels from a source reservoir through the dot network and into the drain reservoir.

Transport through dot networks can be understood by considering the electrochemical potentials of the reservoirs and dot network.[13] The electrochemical potential μ is the energy cost (gain) by adding (removing) an electron.

A source S or drain D reservoir has a higher or lower electrochemical potential respectively. We call the difference in electrochemical potential between the source and the drain the bias window. The bias window is achieved by applying a bias voltage between the source and drain reservoirs. We consider only DC-bias.

The electrochemical potentials of the dot depend on the number of electrons already present in the dot network and the orbitals they occupation. We consider transport through the n-electron ground states of the dot. The electrochemical potential of the n-electron ground state is the energy required to add the nth electron to the dot, and it is defined as

$$\mu(n) = E(n) - E(n-1) \tag{2.2}$$

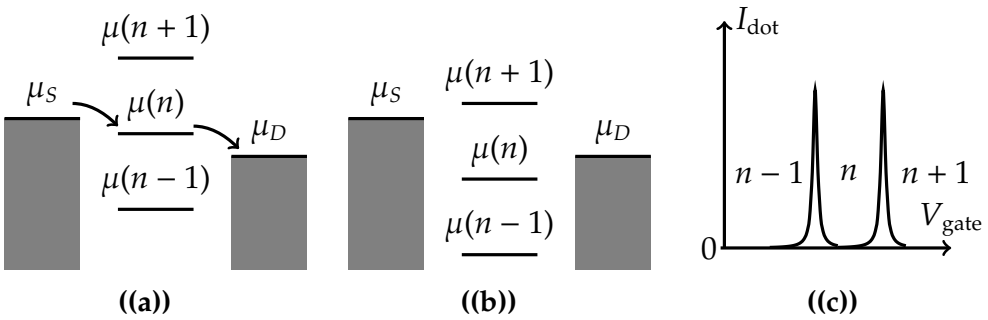

Figure 2.3: Transport through a single dot. In a) the electrochemical potential of n electrons on the dot $\mu(n)$ is within the bias window and electrons may tunnel through the dot. In b) no electrochemical potential is within the bias, and no electrons may tunnel. In c) The current through the dot I_{dot}, in arbitrary units, is plotted as a function of the gate voltage V_{gate} also in arbitrary units. The electron number is fixed between peaks of non-zero current and written between the peaks. The figure is inspired by Fig. 3 in Ref. [10] by Hanson et al.

where $E(n)$ is the energy of the n-electron ground state. To calculate $E(n)$, we use a simplified version of the Constant Interaction model described in Ref. [14]. The model in the reference relies on two assumptions: 1) that the Coulomb interactions of an electron in the dot with all other electrons can be parametrized by a single capacitance, and 2) that the single particle energy spectrum is for non-interacting electrons is unaffected by interactions. The simplification we make is to ignore the capacitive coupling to electrons in the reservoirs. In the simplified model, the energy difference between two consecutive energy levels has two components: The orbital energy of the nth electron and the charging energy which is the energy cost of adding another electron to the dot, due to Coulomb repulsion between electrons in the dot network.

Transport through the dot network is only possible if there is at least one electrochemical potential of the dot network within the bias window such that

$$\mu_S \geq \mu(n) \geq \mu_D \tag{2.3}$$

We sketch this situation for a single dot in Fig. 2.3 (a).

2.2.3 Blockade Phenomena in Dots

In transport through dots, a situation may occur where no current flows even though there is a non-zero bias window. It is called blockade. In this subsection, we describe two blockade phenomena: Coulomb blockade and Pauli blockade.

Coulomb Blockade in a Single Dot

Coulomb blockade occurs at a sufficiently small bias window if non of the electrochemical potentials of the dot is within the bias window. Then the condition in Eq. 2.3 is not fulfilled. As result, no electrons tunnel through the dot. We illustrate this situation in Fig. 2.3 (b). For gate voltages where no electrochemical potential of the dot is within the bias window, the number of electrons is fixed which we illustrate in Fig. 2.3 (c).

Coulomb Blockade in a Double Dot

Coulomb blockade may also occur in transport through a double dot. We label the electrochemical potential levels of the two dots $\mu_{L/R}(n_L, n_R)$ defined as $\mu_L(n_L, n_R) = E_L(n_L, n_R) - E_L(n_L - 1, n_R)$ and $\mu_R(n_L, n_R) = E_R(n_L, n_R) - E_R(n_L, n_R - 1)$ where $n_{L(R)}$ is the number of electrons in the left (right) dot. The condition for electron tunneling through double dots analogous to Eq. 2.3 is

$$\mu_S \geq \mu_L(n_L, n_R) \geq \mu_R(n_L - 1, n_R + 1) \geq \mu_D. \tag{2.4}$$

By tuning the gate voltages of the two dots individually, we can control the number of electrons in each of the dots. We show the electron number in each dot and the current through the dot network as a function of the gate voltages in Fig. 2.4 where we ignore the capacitive coupling between the dots.

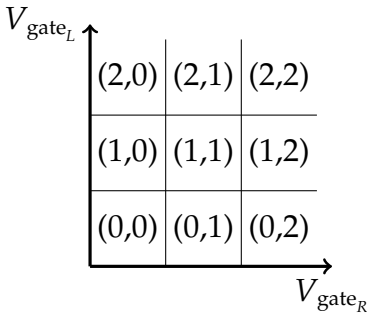

Figure 2.4: Coulomb blockade in a double dot. We plot current through the double dot as a function of the gate voltage on the left and right $V_{\text{gate}_{L/R}}$dot. Non-zero values are marked by black lines. In each square, the electron numbers on both dots are known and labeled (n_L,n_R). We ignore the capacitive coupling between the two dots. The figure is inspired by Fig. 27 in Ref. [10] by Hanson et al.

Pauli blockade

So far we have not considered spin explicitly in the discussion of transport. Pauli exclusion principle states that two electrons in a symmetric spin state cannot occupy the same orbital[15]. This can lead to current rectification in the following situation:

We consider a double dot with the gate voltages tuned such that the right dot is always occupied by at least one electron in the lowest orbital, electrochemical potentials of states with two electrons on the left dot are always out of the bias window, and electrochemical potentials of states with two electrons on the right dot are all outside the bias window except the state where both electrons are in the single particle ground state orbital.

The two electron can only be in the same orbital, if their spin state is the antisymmetric singlet. If the right reservoir is the source, current flows through tunneling events where the population on the right dot alternates between a single electron and two electrons in a singlet spin state. However, if we reverse the bias i.e. make the left reservoir the source, an electron that forms a triplet spin state with the electron on the right dot may tunnel onto the left dot. If it does, it cannot proceed to the right dot and current is blocked. This section is based on Ref. [15] There are proposals on applying a magnetic field to block the singlet state in stead of the triplets[13][16].

2.3 Summary

Quantum computers solve certain problems faster than classical computers. Unfortunately there are still several difficulties to overcome in the experimental realization.

An experimental realization has to fulfill five requirements by DiVincenzo in Ref. [2]. The thesis project addresses two of them, well characterized qubits and the need to initialize the qubits.

The qubit realization we consider is a single electron spin trapped in a quantum dot.

In transport through dots, blockade may occur where no electrons tunnel through the dots even though there is a non-zero bias window. Coulomb blockade occurs when no electrochemical potential of the dots is within the bias window, and Pauli blockade occurs because Pauli's exclusion principle prevents two electrons in a symmetric spin state from occupying the same orbital.

CHAPTER 3

MASTER EQUATION FOR OPEN QUANTUM SYSTEMS

In the next chapter we are interested in the steady state of a triple dot network coupled to reservoirs without considering the state of the reservoirs. In this chapter we set up the formalism to find the density operator of a small system coupled to reservoirs by deriving the master equation for open quantum system.

We start the chapter by discussing density operators, open quantum systems, reduced density operators, and entanglement. In the next section we derive the master equation under the Born and Markov approximations and then we apply it to simple systems to gain intuition for the output of the master equation. Finally, we set up a numerical tool that can perform the same calculations on bigger systems, which will be needed in the next chapter.

Throughout the chapter we refer to the small system of interest simply as the 'system' and the system composed of the small system and the reservoirs as the 'full system'.

3.1 Entanglement and Open Systems

3.1.1 Density Operator for Pure States

This section provides a brief introduction to the density operator formalism, which is needed to describe quantum systems that are coupled to the environment, and thus, as we will see, are not pure states cannot be written as rays in Hilbert space.

We assume that the reader is familiar with pure quantum states described by state vectors, otherwise see Sec. A.1. A pure state $|\psi\rangle$ can also be described by the density operator ρ

$$\rho = |\psi\rangle\langle\psi|. \tag{3.1}$$

The density operator is Hermitian, $\rho = \rho^\dagger$, and positive such that the expectation value of ρ for any state $|\phi\rangle$ fulfills $\langle\phi|\rho|\phi\rangle \geq 0$.[3] The diagonal elements of the density operator are the populations of the basis states normalized to sum to 1. Therefore the density operator has unit trace $\mathrm{Tr}\,\rho = 1$. Furthermore, for pure states

$$\rho^2 = \rho. \tag{3.2}$$

The expectation value of an operator O, using ρ, is calculated as

$$\langle O\rangle = \mathrm{Tr}\,(O\rho). \tag{3.3}$$

The time evolution of the density operator from time t_0 to t is

$$\rho(t) = U(t-t_0)\rho(t_0)U^\dagger(t-t_0). \tag{3.4}$$

The time evolution operator U is unitary, and if the Hamiltonian H of the system is time-independent it is

$$U(t-t_0) = e^{-iH(t-t_0)} \tag{3.5}$$

The infinitesimal time evolution for a time-independent Hamiltonian is given by[17]

$$\dot{\rho}(t) = -i\,[H, \rho(t)] \tag{3.6}$$

3.1.2 Entanglement

The goal of the thesis is to capture an entangled state of two electrons on different quantum dots. In this section, we describe entanglement, which is a quantum correlation between two subsystems that can only be created by interactions of the subsystems. Furthermore, due to the entanglement between the subsystems, the state of each of the subsystems on its own is no longer pure as we shall see below.

We consider two example of Eq. 2.1 to understand the difference between entangled and non-entangled, or separable two-particle states. Both two-particle states are pure. one is entangled and the other is not. In the first example, we choose all coefficients of Eq. 2.1 to be equal

$$\left|\psi\right\rangle = \frac{1}{2}\left(\left|0\right\rangle_1\left|0\right\rangle_2 + \left|0\right\rangle_1\left|1\right\rangle_2 + \left|1\right\rangle_1\left|0\right\rangle_2 + \left|1\right\rangle_1\left|1\right\rangle_2\right). \tag{3.7}$$

In the second example, we choose the non-zero coefficients to be $c_{01} = c_{10} = \frac{1}{\sqrt{2}}$:

$$\left|\psi'\right\rangle = \frac{1}{\sqrt{2}}\left(\left|0\right\rangle_1\left|1\right\rangle_2 + \left|1\right\rangle_1\left|0\right\rangle_2\right). \tag{3.8}$$

We can write $\left|\psi\right\rangle$ as a product of pure states of each of the particles

$$\left|\psi\right\rangle = \frac{1}{\sqrt{2}}\left(\left|0\right\rangle_1 + \left|1\right\rangle_1\right)\frac{1}{\sqrt{2}}\left(\left|0\right\rangle_2 + \left|1\right\rangle_2\right). \tag{3.9}$$

We call $\left|\psi\right\rangle$ a separable state. Another way to determine whether the state is separable is to perform the partial trace over one of the particles, here particle 2, to obtain the reduced density matrix of the other particle, here particle 1:

$$\rho_1 = \mathrm{Tr}_2\,\rho. \tag{3.10}$$

If the density operator of the remaining particle, here 1, describes a pure state, $\left|\psi\right\rangle$ is separable. In our example, we find that

$$\rho_1 = \frac{1}{2}\left(\left|0\right\rangle_1 + \left|1\right\rangle_1\right)\left(\left\langle 0\right|_1 + \left\langle 1\right|_1\right) = \rho_1^2, \tag{3.11}$$

which by Eq. 3.2 lets us conclude that $\left|\psi\right\rangle$ is separable.

For $|\psi'\rangle$ the situation is different. It is not possible to write the state as a product of pure states and the density operator of particle 1 describes a mixed state because

$$\rho_1' = \frac{1}{2}\left(|0\rangle_1 \langle 0|_1 + |1\rangle_1 \langle 1|_1\right) \neq \rho_1'^2. \tag{3.12}$$

The state $|\psi'\rangle$ is entangled and thus not separable.

Two Electrons in Quantum Dots

The following entangled states of two electrons on quantum dots will be important in the next chapter. In this chapter, they serve as examples of how entanglement can be in the orbital or spin part of the state.

Electrons are fermions with spin $s = 1/2$. The total state function of two or more fermions has to be overall antisymmetric under the exchange of any two particles.

We consider a specific example of two electrons occupying distinct orbitals $|\psi_a\rangle$ and $|\psi_b\rangle$, which could be in one or two quantum dots, and we take spin into account. Since the over all state function of two fermions is antisymmetric, either the spatial part or the spin part of the state function is antisymmetric while the other is symmetric. This gives four possible states. Three of them have total spin $s = 1$ and one has total spin $s = 0$. We refer to the three states with $s = 1$ as the triplet states and label them by T_+, T_-, and T_0 for the projection of the total spin along the quantization axis equal to +1,-1, and 0 respectively:

$$|T_+\rangle = \frac{1}{\sqrt{2}}\left(|\psi_a\rangle_1 |\psi_b\rangle_2 - |\psi_b\rangle_1 |\psi_a\rangle_2\right)|\uparrow\rangle_1 |\uparrow\rangle_2 \tag{3.13}$$

$$|T_-\rangle = \frac{1}{\sqrt{2}}\left(|\psi_a\rangle_1 |\psi_b\rangle_2 - |\psi_b\rangle_1 |\psi_a\rangle_2\right)|\downarrow\rangle_1 |\downarrow\rangle_2 \tag{3.14}$$

$$|T_0\rangle = \frac{1}{2}\left(|\psi_a\rangle_1 |\psi_b\rangle_2 - |\psi_b\rangle_1 |\psi_a\rangle_2\right)(|\uparrow\rangle_1 |\downarrow\rangle_2 + |\downarrow\rangle_1 |\uparrow\rangle_2) \tag{3.15}$$

where subscript 1(2) refers to the state of particle 1(2). We refer to the single state with $s = 0$ as the singlet and label it S

$$|S\rangle = \frac{1}{2}\left(|\psi_a\rangle_1 |\psi_b\rangle_2 + |\psi_b\rangle_1 |\psi_a\rangle_2\right)(|\uparrow\rangle_1 |\downarrow\rangle_2 - |\downarrow\rangle_1 |\uparrow\rangle_2)\,. \tag{3.16}$$

If the two electron occupy the same orbital here ψ_a, the spatial part is symmetric and thus the spin state has to be antisymmetric

$$|\psi\rangle_{aa} = \frac{1}{\sqrt{2}}|\psi_a\rangle_1 |\psi_a\rangle_2 (|\uparrow\rangle_1 |\downarrow\rangle_2 - |\downarrow\rangle_1 |\uparrow\rangle_2)\,. \tag{3.17}$$

The states $|T_+\rangle$ and $|T_-\rangle$ have entangled spatial parts and separable spin parts whereas the state $|\psi_{aa}\rangle$ has a separable spatial part and an entangled spin part. The states $|T_0\rangle$ and $|S\rangle$ have entangled spatial and spin parts.

3.1.3 Open Quantum Systems

In this section, we define open quantum systems. In the next section we derive the master equation for the density matrix of an open quantum system.

Pure states, considered in more detail in Sec. A.1, are states of a perfectly isolated, or closed, quantum system. In a realistic set-up, the system of interest will never be perfectly isolated. We call such a system an open quantum system. An open quantum system exchanges energy with its environment. We are interested in the state of the open system alone and not its environment. Due to the exchange of energy, the state of an open quantum system alone is not described by rays in Hilbert space and evolution is not unitary. This section is based on Ref. [3].

We consider the full system, i.e. the open system and its environment, as a closed system. The composed system then follow the rules described in Sec. A.1 and we describe it by the density matrix ρ.

Later on, the environment is a huge reservoir, but we start out with a simple example of a full system consisting of one two-level system coupled to an environment also consisting of a single two-level system. With this example, we want to show that the state of the system alone is in general not a pure state. We consider the system consisting of two two-level systems in Eq. 2.1 with $c_{00} = c_{11} = 0$.

$$|\psi\rangle = c_{01} |0\rangle_1 |1\rangle_2 + c_{10} |1\rangle_1 |0\rangle_2 \tag{3.18}$$

We make the environment i.e. particle 2 inaccessible. We want to know what we can say about the measurement of a particle 1-observable represented by the operator O_1 in this case. The expectation value of an operator is using Eq. A.3

$$\langle O_1\rangle = |c_{01}|^2 \langle 0|_1 O_1 |0\rangle_1 \langle 1|_2 |1\rangle_2 + |c_{10}|^2 \langle 1|_1 O_1 |1\rangle_1 \langle 0|_2 |0\rangle_2 . \tag{3.19}$$

We get the same result if we define the density operator of particle 1 ρ_1 and find the expectation value using Eq. 3.3

$$\rho_1 = |c_{01}|^2 |0\rangle_1 \langle 0|_1 + |c_{10}|^2 |1\rangle_1 \langle 1|_1 \tag{3.20}$$

$$\langle O_1\rangle = \mathrm{Tr}\,(\rho_1 O_1) . \tag{3.21}$$

We may interpret ρ_1 as the density operator as a statistical mixture of the states $|0\rangle$ and $|1\rangle$. We could also obtain ρ_1 by performing the partial trace over particle 2 as in Eq. 3.10.

3.2 Derivation of the Master Equation

In the previous section, we saw that the state of a subsystem is in general a statistical mixture, and we claimed that its time evolution is not unitary. In this section we derive the equation for the time evolution of a small quantum system coupled to a reservoir under the Born and Markov approximations. The equation is known as the master equation. The derivation primarily follows Ref. [17].

We derive the master equation for a quantum dot network connected to electron reservoirs so the reservoirs we consider are fermionic.

A reservoir is a very large system that has many degrees of freedom and a continuous spectrum. Our goal is to obtain the the time evolution of a system S coupled to a reservoir R without keeping track of the time evolution of the reservoir. We know from the previous section that we can find the reduced density matrix of the system by tracing out its environment. In the previous section, the environment was particle 2. In this section it is the reservoir.

We treat the full system as a pure state and describe it by its density operator ρ that evolves in time following

$$\dot{\rho}(t) = -i\left[H, \rho(t)\right]. \tag{3.22}$$

Then in principle we can find the reduced density operator of the system at the time t by tracing out the reservoir

$$\rho_S(t) = \mathrm{Tr}_R\, \rho(t) \tag{3.23}$$

Unfortunately, it is not possible obtain $\rho(t)$ for all t[18]. However, it turns out that it is possible to find an equation for the coarse grained rate of variation of ρ_S with a simple form under certain assumptions and approximations where the most important are the Born approximation and Markov approximation.[17] To provide a better overview, these assumptions and approximations will be listed and discussed in Sec. 3.2.3 and referred back to when applied in the derivation.

The derivation follows these lines: First we transform Eq. 3.22 to the interaction picture, integrate it, and iterate the solution to the integral once. Then we trace out the reservoir and use our approximations and assumptions to simplify the expression for $\rho_S(t)$.

3.2.1 Hamiltonian of the Full System

The Hamiltonian of the full system is

$$H = H_S + H_R + V \tag{3.24}$$

where H_S is the Hamiltonian of the system, H_R is the Hamiltonian of the reservoirs, and V is the interaction between the system and reservoir. We write H_S in a basis of its eigenstates

$$H_S = \sum_{i\sigma} \varepsilon_i c^\dagger_{i\sigma} c_{i\sigma}. \tag{3.25}$$

The exact form of H_R does not affect the general behavior of the subsystem as long as it is large and has a broad, continuous spectrum[18]. More detailed considerations are described in Sec. 3.2.3.

We model the interaction as the simultaneous annihilation of an excitation in the system and creation of an excitation in a reservoir or the reversed process. In our setup however, we couple the triple dot network to several independent reservoirs, so we sum over reservoirs. The interaction term in the Hamiltonian is then

$$V = \sum_r V_r \quad V_r = \sum_\sigma \sum_{ki} \left(g_{ki} c^\dagger_{k\sigma} c_{i,\sigma} + h.c. \right) \tag{3.26}$$

where the index i runs over the discrete levels in the system, σ runs over electron spin, r runs over reservoirs, and k runs over the momentum states in reservoir r.

3.2.2 Interaction Picture

Before integrating Eq. 3.22, we transform it to the interaction picture to eliminate the time evolution from the non-interacting part of the Hamiltonian in Eq. 3.24 H_0. Throughout the thesis a tilde over an operator indicates that it is given in the interaction picture.

In the interaction picture the density operator is

$$\tilde{\rho}(t) = e^{iH_0 t} \rho(t) e^{-iH_0 t} \tag{3.27}$$

and its time evolution is given by

$$\dot{\tilde{\rho}} = -i[\tilde{V}, \tilde{\rho}] \tag{3.28}$$

where $\tilde{V}(t) = e^{iH_0 t} V e^{-iH_0 t}$. For the form of V given in Eq. 3.26, we have

$$\tilde{V}_r(t) = \sum_r \sum_\sigma \sum_{ki} \left(g_{ki} \tilde{c}^\dagger_{k\sigma}(t) \tilde{c}_{i,\sigma}(t) + h.c. \right) \tag{3.29}$$

$$\tilde{c}^\dagger_\alpha(t) = c^\dagger_\alpha e^{i\varepsilon_\alpha t}, \quad \tilde{c}_\alpha(t) = c_\alpha e^{-i\varepsilon_\alpha t}, \tag{3.30}$$

where α is a general index.

3.2.3 Assumptions and Approximations

Before we integrate Eq. 3.28, we go through the assumptions and approximations that we will use throughout the derivation.

Born Approximation

We assume that the interaction V is sufficiently weak such that expansions to second order in V are a good approximations. This is the Born approximation.[19]

Markov approximation

We also assume that there exist three time scales in the problem: T, which is a characteristic time for the evolution of the system due to its coupling to the reservoir, τ_c, which is a characteristic time for the memory of the reservoir, and Δt which is the time scale on which we are interested in the dynamics of the system. We also assume that the timescales relate to each other in the following way

$$T \gg \Delta t \gg \tau_c. \tag{3.31}$$

The assumption that the reservoir memory is very short compared to all other time scales is the Markov approximation.[18]

Assumptions on the Reservoirs

We make the following assumptions regarding the density operator of the reservoirs $\rho_R(t)$ obtained by performing the partial trace over the system such that $\rho_R(t) = \mathrm{Tr}_S\, \rho(t)$:

1) The reservoirs are independent such that the density operator ρ_R describing the reservoirs can be factored into density operators for each reservoir

$$\rho_R = \rho_{R_1} \rho_{R_2} \rho_{R_3} \dots \rho_{R_N}. \tag{3.32}$$

2)We have two types of fermionic reservoirs: sources, with chemical potential $\mu \to \infty$, and drains, with chemical potential $\mu \to 0$ such that all states in a reservoir are either full or empty, respectively. The density operator of a source is then

$$\rho_{\text{Source}} = |1\rangle_{k_1} |1\rangle_{k_2} \dots |1\rangle_{k_N} \langle 1|_{k_N} \dots \langle 1|_{k_2} \langle 1|_{k_1} = \left|\bar{1}\right\rangle \left\langle\bar{1}\right|. \tag{3.33}$$

where the kets and bras in the middle expression is all the $|k\sigma\rangle$ states of the reservoir. In the last equality we defined the short hand notation $\left|\bar{1}\right\rangle \left\langle\bar{1}\right|$ to mean the density operator where all states are full. The density operator of a drain is then

$$\rho_{\text{Drain}} = |0\rangle_{k_1} |0\rangle_{k_2} \dots |0\rangle_{k_N} \langle 0|_{k_N} \dots \langle 0|_{k_2} \langle 0|_{k_1} = \left|\bar{0}\right\rangle \left\langle\bar{0}\right|. \tag{3.34}$$

In the last equality we defined the short hand notation $\left|\bar{0}\right\rangle \left\langle\bar{0}\right|$ to mean the density operator where all states are empty.

3) The reservoir density operator is constant in the interaction picture. The interactions with the system will in principle affect the reservoir, but because the interaction strength is small and the reservoir large, we assume that $\tilde{\rho}_R(t)$ is constant in the interaction picture

$$\tilde{\rho}_R(t) \simeq \tilde{\rho}_R(0) = \rho_R. \tag{3.35}$$

4) Each reservoir is in a stationary state with respective to the reservoir Hamiltonian H_R. Therefore ρ_R and H_R commute

$$[H_R, \rho_R] = 0. \tag{3.36}$$

Hence ρ_R can be written as a statistical mixture of eigenstate to H_R.

5) Averages of system operators: The one-time average of $c_{k\sigma}^{(\dagger)}$ is zero

$$\text{Tr}_R \left(\tilde{c}_{k_R\sigma}^{(\dagger)}(t)\rho_R\right) = 0. \tag{3.37}$$

This is not really and assumption but follows from assumption 2) where the density operators of source and drain reservoirs are specified. We do assume that the two-time averages of system operators $c_{k\sigma}^{(\dagger)}$ decays rapidly or in other words that the reservoir memory is very short. In the interaction picture the non-zero two-time averages are

$$\text{Tr}_R \left(c_{k\sigma}^\dagger(t) c_{k\sigma}(t')\rho_{\text{Source}}\right) = \text{Tr}_R \left(c_{k\sigma}^\dagger c_{k\sigma}\rho_{\text{Source}}\right) e^{i\omega_k(t-t')} = e^{i\omega_k(t-t')} \tag{3.38}$$

$$\text{Tr}_R \left(c_{k\sigma}(t) c_{k\sigma}^\dagger(t')\rho_{\text{Drain}}\right) = \text{Tr}_R \left(c_{k\sigma} c_{k\sigma}^\dagger\rho_{\text{Drain}}\right) e^{-i\omega_k(t-t')} = e^{-i\omega_k(t-t')} \tag{3.39}$$

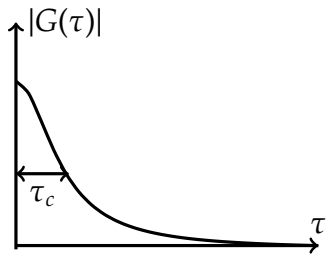

Figure 3.1: A schematic plot of $|G(\tau)|$. The characteristic time of the memory of the reservoir is marked by τ_c.

We will encounter the k-sum over the traces weighted with the coupling strength to the reservoir g_k. We define this as the function G

$$G(\tau) = \sum_k |g_k|^2 e^{i\omega_k(\tau)} \quad \tau = t - t'. \tag{3.40}$$

The two time average, $G(\tau)$, is a sum of complex exponentials oscillating at the frequencies ω_k. Since the reservoir has a broadband spectrum destructive interference occurs for τ large enough. In figure Fig. 3.1 we plot a potential form of $|G(\tau)|$. The characteristic time for the reservoir memory is τ_c.

3.2.4 Integration and Iteration

We integrate Eq. 3.28 from t to Δt and move $\tilde{\rho}(t)$ to the other side of the equation

$$\tilde{\rho}(t + \Delta t) = \tilde{\rho}(t) - i \int_t^{t+\Delta t} \mathrm{d}t' \left[\tilde{V}(t'), \tilde{\rho}(t')\right]. \tag{3.41}$$

This equation can be solved by iteration. We use the Born approximation described in Sec. 3.2.3, so we iterate once to obtain

$$\begin{aligned}\tilde{\rho}(t + \Delta t) - \tilde{\rho}(t) = &- i \int_t^{t+\Delta t} \mathrm{d}t' \left[\tilde{V}(t'), \tilde{\rho}(t)\right] \\ &- \int_t^{t+\Delta t} \mathrm{d}t' \int_t^{t'} \mathrm{d}t'' \left[\tilde{V}(t'), \left[\tilde{V}(t''), \tilde{\rho}(t'')\right]\right].\end{aligned} \tag{3.42}$$

3.2.5 Tracing out Source Reservoirs

In the following we trace out the reservoirs. Here we consider source reservoirs in the evaluation. The evaluation for drain reservoirs is similar and the results are presented in Sec. 3.2.7.

We trace out the reservoirs to obtain an expression for the density operator of the system

$$\begin{aligned}\tilde{\rho}_S(t+\Delta t) - \tilde{\rho}_S(t) = &- i \int_t^{t+\Delta t} \mathrm{d}t' \, \mathrm{Tr}_R \left[\tilde{V}(t'), \tilde{\rho}(t)\right] \\ &- \int_t^{t+\Delta t} \mathrm{d}t' \int_t^{t'} \mathrm{d}t'' \, \mathrm{Tr}_R \left[\tilde{V}(t'), \left[\tilde{V}(t''), \tilde{\rho}(t'')\right]\right], \end{aligned} \tag{3.43}$$

where the left hand side follows from Eq. 3.23.

By Eq. 3.37 and Eq. 3.29, the first term on the right hand side is zero. For V sufficiently weak and $T \gg \Delta t \implies T \gg t'' - t$, it is reasonable to replace $\tilde{\rho}(t'')$ by $\tilde{\rho}(t)$. We introduce the notation $\tilde{\rho}_S(t+\Delta t) - \tilde{\rho}_S(t) = \Delta\tilde{\rho}_S(t)$ and divide by Δt on both hand sides

We have now obtained the coarse grained rate of variation for the system:

$$\frac{\Delta\tilde{\rho}_S(t)}{\Delta t} = \frac{-1}{\Delta t} \int_t^{t+\Delta t} \mathrm{d}t' \int_t^{t'} \mathrm{d}t'' \, \mathrm{Tr}_R \left[\tilde{V}(t'), \left[\tilde{V}(t''), \tilde{\rho}(t)\right]\right]. \tag{3.44}$$

To evaluate the reservoir traces, we use that we can write the density operator of the full system as

$$\rho(t) = \mathrm{Tr}_R(\rho(t)) \otimes \mathrm{Tr}_S(\rho(t)) + \rho_{\mathrm{corr}}(t). \tag{3.45}$$

The last term gives the correlation between the system and the reservoirs at time t. Because correlations die off on the timescale of τ_c and we are interested in the dynamics on the time scale $\Delta t \gg \tau_c$, the correlations present at time t do not contribute much to the evolution over Δt, and we ignore them

$$\rho(t) \simeq \mathrm{Tr}_R(\rho(t)) \otimes \mathrm{Tr}_S(\rho(t)). \tag{3.46}$$

We evaluate the reservoir traces in detail for source reservoirs and state the result for drain reservoirs. Writing out the commutators results in four

traces to evaluate

$$\mathrm{Tr}_R\left(\tilde{V}(t')\tilde{V}(t'')\tilde{\rho}(t)\right) \tag{3.47}$$

$$\mathrm{Tr}_R\left(\tilde{V}(t')\tilde{\rho}(t)\tilde{V}(t'')\right) \tag{3.48}$$

$$\mathrm{Tr}_R\left(\tilde{V}(t'')\tilde{\rho}(t)\tilde{V}(t')\right) \tag{3.49}$$

$$\mathrm{Tr}_R\left(\tilde{\rho}(t)\tilde{V}(t'')\tilde{V}(t')\right) \tag{3.50}$$

As presented in Eq. 3.29, the interaction contains a sum over reservoirs. When we multiply out each trace we thus obtain terms with two operators acting on different reservoirs and terms where both operators act on the same reservoir. However, the former terms vanish due to Eq. 3.37 for each reservoir.

Only taking terms where all reservoir operators act on the same reservoir into account, each trace contains four terms. However, only one of them is non-zero. For Eq. 3.47 the only non-zero term is

$$\sum_{kk'}\sum_{\sigma\sigma'}\sum_{il} g_{ki}g^*_{k'l}c_{i\sigma}c^\dagger_{l\sigma'}\tilde{\rho}_S(t)\underbrace{\mathrm{Tr}_R\left(c^\dagger_{k\sigma}c_{k'\sigma'}\left|\bar{1}\right\rangle\left\langle\bar{1}\right|\right)}_{\delta_{kk'}\delta_{\sigma\sigma'}}e^{-i\omega_i t'+i\omega_l t''+i\omega_k t'-i\omega_{k'}t''}, \tag{3.51}$$

where $\left|\mu\right\rangle$ is a complete basis of the reservoir. We reduce the summation with the Kronecker delta's

$$=\sum_{k\sigma}\sum_{il} g_{ki}g^*_{kl}c_{i\sigma}c^\dagger_{l\sigma}\tilde{\rho}_S(t)e^{-i\omega_i t'+i\omega_l t''+i\omega_k(t'-t'')} \tag{3.52}$$

For Eq. 3.48 the only non-zero term is

$$\sum_{k\sigma}\sum_{il} g^*_{ki}g_{kl}c^\dagger_{i\sigma}\tilde{\rho}_S(t)c_{l\sigma}e^{i\omega_i t'-i\omega_l t''-i\omega_k(t'-t'')} \tag{3.53}$$

For Eq. 3.49 the only non-zero term is

$$\sum_{k\sigma}\sum_{il} g_{ki}g^*_{kl}c^\dagger_{l\sigma}\tilde{\rho}_S(t)c_{i\sigma}e^{-i\omega_i t'+i\omega_l t''+i\omega_k(t'-t'')} \tag{3.54}$$

For Eq. 3.50 the only non-zero term is

$$\sum_{k\sigma}\sum_{il} g^*_{ki}g_{kl}\tilde{\rho}_S(t)c_{l\sigma}c^\dagger_{i\sigma}e^{i\omega_i t'-i\omega_l t''-i\omega_k(t'-t'')} \tag{3.55}$$

3.2.6 Performing the Time Integration

We substitute Eq. 3.52-Eq. 3.55 into Eq. 3.44 and change the variables of integration from t' and t'' to t' and $\tau = t' - t''$:[17]

$$\int_t^{t+\Delta t} \mathrm{d}t' \int_t^{t'} \mathrm{d}t'' = \int_0^{\Delta t} \mathrm{d}\tau \int_{t+\tau}^{t+\Delta t} \mathrm{d}t' \tag{3.56}$$

Eq. 3.44 becomes

$$\begin{aligned}\frac{\Delta\tilde{\rho}(t)}{\Delta t} = -\sum_{k\sigma}\sum_{il}\Big[& g_{ki}g_{kl}^{*}\left(c_{i\sigma}c_{l\sigma}^{\dagger}\tilde{\rho}_S(t) - c_{l\sigma}^{\dagger}\tilde{\rho}_S(t)c_{i\sigma}\right) \\ & \times \int_0^{\Delta t}\mathrm{d}\tau e^{-i(\omega_l-\omega_k)\tau}\frac{1}{\Delta t}\int_{t+\tau}^{t+\Delta t}\mathrm{d}t' e^{-i(\omega_i-\omega_l)t'} \\ & + g_{ki}^{*}g_{kl}\left(\tilde{\rho}_S(t)c_{l\sigma}c_{i\sigma}^{\dagger} - c_{i\sigma}^{\dagger}\tilde{\rho}_S(t)c_{l\sigma}\right) \\ & \times \int_0^{\Delta t}\mathrm{d}\tau e^{i(\omega_l-\omega_k)\tau}\frac{1}{\Delta t}\int_{t+\tau}^{t+\Delta t}\mathrm{d}t' e^{i(\omega_i-\omega_l)t'}\Big]\end{aligned} \tag{3.57}$$

We recognize $G(\tau)$ that we defined in Eq. 3.40 in the τ-integral and because we know it decays in a characteristic time τ_c much shorter than Δt we introduce only a small error by extending the upper limit on the τ-integral to ∞ and the lower limit on the t'-integral to t. We solve the t'-integral

$$\begin{aligned}\int_t^{t+\Delta t}\mathrm{d}t' e^{\pm i(\omega_i-\omega_l)t'} &= e^{\pm i(\omega_i-\omega_l)t}\frac{e^{\pm i(\omega_i-\omega_l)\Delta t/2}}{\pm i\left(\omega_i-\omega_l\right)\Delta t}\left(e^{\pm i(\omega_i-\omega_l)\Delta t/2} - e^{\mp i(\omega_i-\omega_l)\Delta t/2}\right) \\ &= e^{\pm i(\omega_i-\omega_l)t}e^{\pm i(\omega_i-\omega_l)\Delta t/2}\frac{\sin\left[\left(\omega_i-\omega_l\right)\Delta t/2\right]}{\left(\omega_i-\omega_l\right)\Delta t/2} = e^{\pm i(\omega_i-\omega_l)t}e^{\pm ix}\frac{\sin x}{x} \\ & \qquad x = \left(\omega_i-\omega_l\right)\Delta t/2\end{aligned} \tag{3.58}$$

and get the sinc-function modified by a complex exponential. This function decreases rapidly for increasing $|x|$. This means that only terms with $|\omega_i - \omega_l| \ll \Delta t$ contribute to the master equation. We use the strict requirement $\omega_i = \omega_l$ in the rest of the derivation. We see that terms which couple levels of very different energy do not contribute much to the rate of variation. This situation is similar to the situation in closed quantum system described in Sec. A.5 where an interaction V_{ij} that directly couples two levels i and j has a small effect if $V_{ij} \ll \left|E_i - E_j\right|$.

We now solve the τ-integral with the extended boundary[20]

$$\int_0^{\infty}\mathrm{d}\tau e^{\pm i(\omega_l-\omega_k)\tau} = \pi\delta\left(\omega_l-\omega_k\right) \pm iPV\left(\frac{1}{\left(\omega_l-\omega_k\right)}\right) \tag{3.59}$$

where PV is the principal value which we ignore here.[19] Now we obtain the final form of the coarse grained rate of variation of the systems density operator in the interaction picture due to the coupling to a source reservoir with a relabeling of the summation indices

$$\frac{\Delta\tilde{\rho}(t)}{\Delta t} = {\sum_{il}}' \gamma_r c_{l\sigma}^\dagger \tilde{\rho}_S(t) c_{i\sigma} e^{-i(\omega_i-\omega_l)t} - \frac{\gamma_r}{2}\{c_{i\sigma}c_{l\sigma}^\dagger, \tilde{\rho}_S(t)\}e^{-i(\omega_i-\omega_l)t} \tag{3.60}$$
$$\gamma_r = \sum_{k\sigma} 2\pi \left|g_k\right|^2 \delta(\omega_l - \omega_k)$$

assuming $g_{ki} = g_{kl}$ and where the prime on the summation means that it is restricted to terms where $\omega_i = \omega_l$.

3.2.7 Contribution Drains

We go through the same calculations for a drain reservoir using the drain density operator from Eq. 3.34 to evaluate the traces in Eq. 3.47-Eq. 3.50. The result is

$$\frac{\Delta\tilde{\rho}(t)}{\Delta t} = {\sum_{il}}' \gamma_r c_{l\sigma} \tilde{\rho}_S(t) c_{i\sigma}^\dagger e^{i(\omega_i-\omega_l)t} - \frac{\gamma_r}{2}\{c_{i\sigma}^\dagger c_{l\sigma}, \tilde{\rho}_S(t)\}e^{i(\omega_i-\omega_l)t} \tag{3.61}$$
$$\gamma_r = \sum_{k\sigma} 2\pi \left|g_k\right|^2 \delta(\omega_l - \omega_k)$$

also assuming $g_{ki} = g_{kl}$.

3.2.8 Final Form

We combine the contributions from sources and drains and put the master equation into

$$\frac{\Delta\tilde{\rho}_S(t)}{\Delta t} = \sum_r^{\text{Sources}} {\sum_{il}}' \gamma_r c_{l\sigma}^\dagger \tilde{\rho}_S(t) c_{i\sigma} e^{-i(\omega_i-\omega_l)t} - \frac{\gamma_r}{2}\{c_{i\sigma}c_{l\sigma}^\dagger, \tilde{\rho}_S(t)\}e^{-i(\omega_i-\omega_l)t}$$
$$+ \sum_r^{\text{Drains}} {\sum_{il}}' \gamma_r c_{l\sigma} \tilde{\rho}_S(t) c_{i\sigma}^\dagger e^{i(\omega_i-\omega_l)t} - \frac{\gamma_r}{2}\{c_{i\sigma}^\dagger c_{l\sigma}, \tilde{\rho}_S(t)\}e^{i(\omega_i-\omega_l)t} \tag{3.62}$$

We transform back to the Schrödinger picture using Eq. 3.27

$$\frac{\Delta\rho_S(t)}{\Delta t} = -i[H,\rho_S(t)] + \sum_r^{\text{Sources}} {\sum_{il}}' \gamma_r c_{l\sigma}^\dagger \rho_S(t) c_{i\sigma} - \frac{\gamma_r}{2}\{c_{i\sigma}c_{l\sigma}^\dagger, \rho_S(t)\} + \sum_r^{\text{Drains}} {\sum_{il}}' \gamma_r c_{l\sigma} \rho_S(t) c_{i\sigma}^\dagger - \frac{\gamma_r}{2}\{c_{i\sigma}^\dagger c_{l\sigma}, \rho_S(t)\} \quad (3.63)$$

To make the notation more compact, we define the Lindblad operators which for a non-degenerate level coupled to a source with coupling strength γ_r is $L_k = \sqrt{\gamma_r}c^\dagger$ and for a non-degenerate level coupled to a drain with coupling strength γ_r is $L_k = \sqrt{\gamma_r}c$. The Lindblad operator for degenerate levels i and j coupled to the same source reservoir with coupling strength γ_r is $L_k = \sqrt{\gamma_r}(c_{i\sigma}^\dagger + c_{j\sigma}^\dagger)$ and for i and j coupled to the same drain reservoir is $L_k = \sqrt{\gamma_r}(c_{i\sigma} + c_{j\sigma})$

$$\frac{\Delta\rho_S(t)}{\Delta t} = -i[H_0,\rho_S(t)] + \sum_r \sum_m L_{mr}\rho_S(t)L_{mr}^\dagger - \frac{1}{2}\{L_{mr}^\dagger L_{mr}, \rho_S(t)\} \quad (3.64)$$

The first term on the right hand side represents the unitary evolution of the system. The second term represents the possible jumps that may occur in the system due to the interaction with the reservoir such as an electron leaking into or out of the system and the third term ensures normalization.

3.3 Analysis of One- and Two-level Systems Coupled to Reservoirs

In the previous section, we derived the master equation for a small system coupled to reservoirs. Before we apply the master equation to the triple dot network in the next chapter, we find it helpful to apply it to simpler systems, so we can check that its output is in accordance with our intuition. In this section, we apply the master equation to a one-level system coupled to a source and a drain and a two-level system coupled to a drain reservoir.

3.3.1 One Level Coupled to a Source and a Drain

The system, which could be a quantum dot with a single orbital, is described by the Hamiltonian $H = \varepsilon c^\dagger c$. It is coupled to a source reservoir with coupling strength γ_{in} and a drain reservoir with coupling strength γ_{out}, see Fig. 3.2.

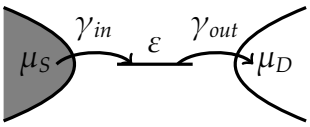

Figure 3.2: One discrete level indicated by a horizontal line is coupled to a source reservoir to the left with coupling strength γ_{in} and a drain reservoir to the right with coupling strength γ_{out}.

The Hilbert space is two dimensional and spanned by the states $\{|1\rangle, |0\rangle\}$ indicating the occupancy of the level. Operators are also given in that basis. The Lindblad operators are

$$L_1 = \begin{pmatrix} 0 & \sqrt{\gamma_{in}} \\ 0 & 0 \end{pmatrix} \quad L_2 = \begin{pmatrix} 0 & 0 \\ \sqrt{\gamma_{out}} & 0 \end{pmatrix}, \tag{3.65}$$

where L_1 transfers population from the source to the level and L_2 transfers population from the level to the drain. In Sec. 3.2.8, we described how the first non-Hermitian term corresponds to jumps and the second ensures that the density operator remains normalized. Here we show it by calculating the terms $L_1 \rho L_1^\dagger$ and $\{L_1^\dagger L_1, \rho\}$ explicitly.

$$L_1 \rho L_1^\dagger = \begin{pmatrix} \gamma_{in}\rho_{22} & 0 \\ 0 & 0 \end{pmatrix} \tag{3.66}$$

$$-\frac{1}{2}\{L_1^\dagger L_1, \rho\} = -\frac{\gamma_{in}}{2}\begin{pmatrix} 0 & \rho_{12} \\ \rho_{21} & 2\rho_{22} \end{pmatrix} \tag{3.67}$$

The $L_1 \rho L_1^\dagger$ term correspond to an electron leaking into the system and the second term makes sure that the density operator remains normalized. By Eq. 3.64, the master equation is

$$\begin{pmatrix} \dot{\rho}_{11} & \dot{\rho}_{12} \\ \dot{\rho}_{21} & \dot{\rho}_{22} \end{pmatrix} = \begin{pmatrix} \gamma_{in}\rho_{22} - \gamma_{out}\rho_{11} & -\left[\frac{1}{2}(\gamma_{in} + \gamma_{out}) + i\varepsilon\right]\rho_{12} \\ \left[-\frac{1}{2}(\gamma_{in} + \gamma_{out}) + i\varepsilon\right]\rho_{21} & \gamma_{out}\rho_{11} - \gamma_{in}\rho_{22} \end{pmatrix}. \tag{3.68}$$

The steady state solution ρ_{ss} fulfills $\dot{\rho}_{ss} = 0$. It is

$$\rho_{\text{ss}} = \begin{pmatrix} \frac{1}{1+\left(\frac{\gamma_{out}}{\gamma_{in}}\right)} & 0 \\ 0 & \frac{1}{1+\left(\frac{\gamma_{in}}{\gamma_{out}}\right)} \end{pmatrix}. \tag{3.69}$$

We check that the solution matches our expectations for three specific cases: 1) Setting $\gamma_{out} = 0$ corresponds to the electron being trapped in the

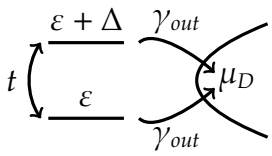

Figure 3.3: Two discrete levels indicated by horizontal lines coupled to a drain reservoir with coupling strength γ_{out}, and to each other with strength t.

level, and we expect the steady state to be a fully occupied level. 2) On the other hand turning off the coupling to the source is achieved for $\gamma_{in} = 0$, and we expect the steady state to be a complete empty level. 3) Finally, if the couplings are equal, we expect the steady state to be a statistical mixture of full and empty with equal probability. These special cases of Eq. 3.69 are evaluated to be

$$\rho_{\text{ss.},\gamma_{in}=0} = \begin{pmatrix} 0 & 0 \\ 0 & 1 \end{pmatrix}, \quad \rho_{\text{ss},\gamma_{out}=0} = \begin{pmatrix} 1 & 0 \\ 0 & 0 \end{pmatrix}, \quad \rho_{\text{ss},\gamma_{in}=\gamma_{out}} = \begin{pmatrix} \frac{1}{2} & 0 \\ 0 & \frac{1}{2} \end{pmatrix} \tag{3.70}$$

which is exactly as expected. For the simplest case the steady state of the system predicted by the master equation is in full accordance with our intuition.

3.3.2 Two Levels Coupled to a Drain

For two levels coupled to one drain, the appropriate Lindblad operators will be linear combinations of the system operators if the levels are degenerate, as described in Sec. 3.2.8. To illustrate the effect of interference, we study a two-level system as shown in Fig. 3.3. The two levels have energies ε and $\varepsilon + \Delta$ respectively. We choose to limit total number of electrons in the system to 0 or 1, because it is sufficient to show the effect of interference. We choose the basis $\{|1,0\rangle, |0,1\rangle, |0,0\rangle\}$ in which the Hamiltonian is

$$H = \begin{pmatrix} \varepsilon & 0 & 0 \\ 0 & \varepsilon + \Delta & 0 \\ 0 & 0 & 0 \end{pmatrix} \tag{3.71}$$

Both levels couple to a drain with the same coupling strength γ_{out}. The Lindblad operators are

$$L_1 = \begin{pmatrix} 0 & 0 & 0 \\ 0 & 0 & 0 \\ \sqrt{\gamma_{out}} & 0 & 0 \end{pmatrix}, \quad L_2 = \begin{pmatrix} 0 & 0 & 0 \\ 0 & 0 & 0 \\ 0 & \sqrt{\gamma_{out}} & 0 \end{pmatrix} \tag{3.72}$$

where L_1 transfers population from the level with energy ε to the drain and L_2 transfers population from the level with energy $\varepsilon + \Delta$ to the drain. If we do not take interference into account, the master equation and its steady state solution are

$$\begin{pmatrix} \dot{\rho}_{11} & \dot{\rho}_{12} & \dot{\rho}_{13} \\ \dot{\rho}_{21} & \dot{\rho}_{22} & \dot{\rho}_{23} \\ \dot{\rho}_{31} & \dot{\rho}_{32} & \dot{\rho}_{33} \end{pmatrix} = \begin{pmatrix} -\gamma_{out}\rho_{11} & [-\gamma_{out} + i\Delta]\,\rho_{12} & -\left[\frac{\gamma_{out}}{2} + i\varepsilon\right]\rho_{13} \\ -\left[\gamma_{out} + i\Delta\right]\rho_{21} & -\gamma_{out}\rho_{22} & -\left[\frac{\gamma_{out}}{2} + i\,(\varepsilon + \Delta)\right]\rho_{23} \\ \left[\frac{\gamma_{out}}{2} - i\varepsilon\right]\rho_{31} & \left[-\frac{\gamma_{out}}{2} + i\,(\varepsilon + \Delta)\right]\rho_{32} & \gamma_{out}\,(\rho_{11} + \rho_{22}) \end{pmatrix} \tag{3.73}$$

$$\rho_{ss} = \begin{pmatrix} 0 & 0 & 0 \\ 0 & 0 & 0 \\ 0 & 0 & 1 \end{pmatrix} \tag{3.74}$$

If we take the interference into account for $\Delta = 0$, $L_1 + L_2$ enters the master equation and it becomes

$$\dot{\rho} = \begin{pmatrix} \frac{-\gamma_{out}}{2}\left[2\rho_{11} + \rho_{12} + \rho_{21}\right] & -\frac{\gamma_{out}}{2}\left[2\rho_{12} + \rho_{11} + \rho_{22}\right] & -\left[i\varepsilon + \frac{\gamma_{out}}{2}\right]\rho_{13} - \frac{\gamma_{out}}{2}\rho_{23} \\ -\frac{\gamma_{out}}{2}\left[2\rho_{21} + \rho_{11} + \rho_{22}\right] & -\frac{\gamma_{out}}{2}\left[2\rho_{22} + \rho_{12} + \rho_{21}\right] & -\left[i\varepsilon + \frac{\gamma_{out}}{2}\right]\rho_{23} - \frac{\gamma_{out}}{2}\rho_{13} \\ \left[-i\varepsilon + \frac{\gamma_{out}}{2}\right]\rho_{31} - \frac{\gamma_{out}}{2}\rho_{32} & \left[i\varepsilon - \frac{\gamma_{out}}{2}\right]\rho_{32} - \frac{\gamma_{out}}{2}\rho_{31} & \gamma_{out}\,(\rho_{11} + \rho_{22} + \rho_{12} + \rho_{21}) \end{pmatrix}. \tag{3.75}$$

We find two independent steady state solutions

$$\rho_{ss_1} = \begin{pmatrix} 0 & 0 & 0 \\ 0 & 0 & 0 \\ 0 & 0 & 1 \end{pmatrix}, \quad \rho_{ss_2} = \begin{pmatrix} \frac{1}{2} & -\frac{1}{2} & 0 \\ -\frac{1}{2} & \frac{1}{2} & 0 \\ 0 & 0 & 0 \end{pmatrix}. \tag{3.76}$$

We can understand why there are two steady state solution by considering the problem in a basis of the symmetric and antisymmetric combination of the two levels in the system. Then $L_1 + L_2$ couples to the symmetric combination only. This way, the antisymmetric combination is decoupled from the drain and it can thus get stuck. The steady state solution in Eq. 3.76 is exactly the density operator of the antisymmetric combination.

3.4 A Numerical Tool for Solving the Master Equation

In the next chapter, we will perform the same type of calculation for a larger system and many parameter configurations, so we need a numerical tool to set up the master equation and find the steady state solution.

The numerical tool consists of two parts. The first part contains functions that can be used to set up the master equation and find the steady state solution for general systems. The systems can have arbitrarily many discrete levels coupled to each other and the reservoirs in any way. The second part contains information on the physics of the specific system. The information is included through the single particle Hamiltonian, interactions between the particles in the systems, the number of reservoirs, the coupling strength and whether interference is taken into account in the coupling.

The first part is written by Professor Flensberg, who is a secondary advisor on the project. In his version, cross terms for degenerate levels are ignored in Eq. 3.63 such that the Lindblad operators in Eq. 3.64 always equal the square root of the coupling strength times one annihilation or creation operator. We modify it such that the Lindblad operators can also be linear combinations of creation and annihilation operators of the system and such that it can compute steady state populations. The code is available upon request.

We will not go into detail with the various functions of the code, but one step is essential: The steady state is found by transforming Eq. 3.64 to the following form

$$\underline{\dot{\rho}} = \underline{\underline{L}}\,\underline{\rho} \tag{3.77}$$

where $\underline{\rho}$ is a vector containing the elements of ρ and finding the null space of the matrix $\underline{\underline{L}}$.

In this thesis, we use three different versions of the second part of the numerical tool: One for the one-level system, one for the two-level system, and one for the triple dot network described in the next chapter. They are all written by the author. The code for the one- and two-level systems and for the triple dot network is available upon request.

As a minimal test of the numerical tool, we apply it to the one- and two-level systems described in Sec. 3.3.1 and Sec. 3.3.2 and obtain the same results.

3.5 Summary

In this chapter we derived the master equation of an open quantum system under the Born and Markov approximations. We used the master equation to find the steady state of a one-level system coupled to a source and a drain and of a two-level system coupled to a drain. We obtained results in accordance with our intuition. In the next chapter we want to find the steady state for a larger system, and we thus need a numerical tool to set up the master equation and find the steady state solutions. We tested the tool on the simple systems and obtained the same as in our analytical calculations.

CHAPTER 4

Triple Dot Network

The aim of this thesis is to investigate whether we can tune the parameters of a linear triple dot network and its coupling to source and drain reservoirs such that the steady state of the network has a large population of the singlet state with one electron on each of the outer dots.

In this chapter, we set up a model for transport in a triple dot network that may have the ability to hold a large population of the desired spin state in its steady state. We investigate the parameter dependence of the steady state singlet population in two ways: by a perturbative approach and by numerically computing the steady state of the master equation for the triple dot network.

There are other works on using triple quantum dots for qubit realization in different ways. [21][22][23]

4.1 Model of the Triple Dot Network

We consider a triple dot network that consists of three quantum dots in a row coupled to three reservoirs. Each of the outer dots is coupled to a source reservoir with electrochemical potential μ_S and the middle dot to a drain reservoir with electrochemical potential μ_D. The incoming and outgoing rates are γ_{in} and γ_{out}, respectively. Two neighboring dots are weakly coupled with a tunneling coefficient t. A diagram of the setup in shown in Fig. 4.1.

We assume that the bias window is such that only states with two or fewer electrons in the network can get populated. The level spacings and

charging energies of the dots further restrict which two-electron states are allowed in the network. We take the outer dots to be small enough that the level spacing and charging energy are so large that only states with maximally one electron on each of the outer dots in the ground state are allowed. We take the middle dot to be significantly bigger than the outer dots so its level spacing is smaller, see Sec. 2.2.1. The larger size of the middle dot also leads to a smaller charging energy. In our description of the dot network, we take states with up to two electrons on the middle dot in the ground state or first excited state into account. We assume that the electrochemical potential of the source reservoirs is much bigger than those of all allowed states and much smaller than the electrochemical potentials of all excluded states.

We label the ground states of the outer dots by their energies, ε_L and ε_R, and the ground state and first excited state of the middle dot, ε_M and $\varepsilon_{M+\Delta}$. Each of the four orbitals is spin degenerate. We assume $T = 0$ so level broadening does not occur due to temperature. It does occur due to the coupling to reservoirs, but we ignore this effect until Sec. 4.1.3.

In the following subsections, we discuss restrictions on the Hilbert space, set up a Hamiltonian for the system, introduce the outgoing rate as a phenomenological parameter, and discuss the broadening of the energy levels coupled to the drain reservoir mentioned above. Finally, we argue that it should be possible to capture the singlet state on the outer dots using a blockade phenomenon in which the singlet is blocked and the triplets leak out of the network rapidly.

4.1.1 Allowed Many-body States

Since all four orbitals in the triple dot network are spin degenerate, we have eight single particle states which can be occupied or empty in all combinations. With the assumptions on the bias window described in the previous section, we end up with a 35-dimensional Hilbert space.

In equations, we use two different notations for the states in order to enhance clarity in each given context. We order the single particle state basis in this way: $\{|L\uparrow\rangle, |L\downarrow\rangle, |M\uparrow\rangle, |M\downarrow\rangle, |M+\Delta\uparrow\rangle, |M+\Delta\downarrow\rangle, |R\uparrow\rangle, |R\downarrow\rangle\}$ Then using the first notation the many body state kets are written as

$$\begin{aligned} \big|\psi\big\rangle &= \big|n_{L\uparrow}, n_{L\downarrow}, n_{M\uparrow}, n_{M\downarrow}, n_{M+\Delta,\uparrow}, n_{M+\Delta,\downarrow}, n_{R\uparrow}, n_{R\downarrow}\big\rangle \\ n_i &= 0, 1, \quad \sum_i n_i \leq 2. \end{aligned} \tag{4.1}$$

For some purposes, we find it clearer to write only the occupation number of a given orbital in the ket of two-electron states and give the spin state

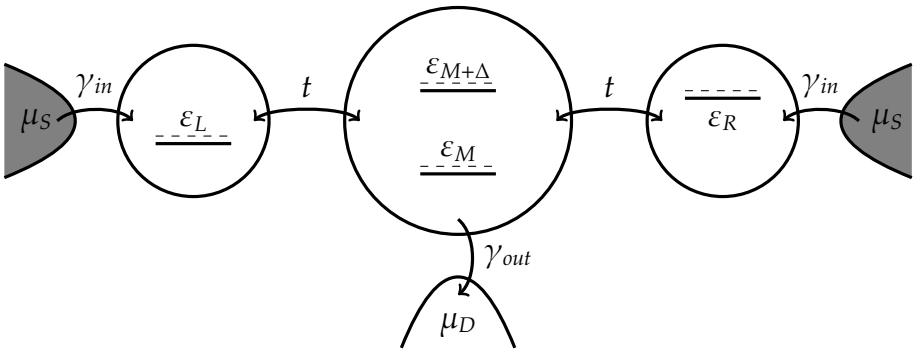

Figure 4.1: Schematic drawing of the triple dot network. The triple dot network consists of three dots drawn as circles. The bigger, middle dot is coupled to the drain labeled with its electrochemical potential μ_D. The coupling results in an outgoing rate γ_{out}. The two smaller dots are each coupled to a source labeled with their electrochemical potential μ_S. The coupling results in an incoming rate γ_{in}. Due to the size of the bias window, there is one accessible orbital on each of the outer dots with energy ε_L and ε_R respectively. On the middle dot there are two accessible orbitals with energy ε_M and $\varepsilon_{M+\Delta}$. The orbitals are spin degenerate and drawn as black lines and dashed lines to mark the spin degeneracy. The inter dot tunneling coefficient is t.

as a label. In this, the second, notation, a state is written as

$$\begin{aligned} |\psi\rangle &= |n_L, n_M n_{M+\Delta}, n_R\rangle^{\chi} \\ n_i &= 0, 1, 2 \\ \chi &= S, T_-, T_0, T_+. \end{aligned} \tag{4.2}$$

As a shorthand, we will label states by the string of the four numbers n_i above. As an example, the "1001-singlet" state refers to the singlet state with $n_L = 1, n_M = 0, n_{M+\Delta} = 0$, and $n_R = 1$.

4.1.2 Hamiltonian

In this subsection, we begin with a phenomenological discussion of the terms appearing in the Hamiltonian and the processes that they describe. In a later subsection we will employ a specific model to estimate the sizes of the terms in the Hamiltonian. We set up the Hamiltonian H of the isolated triple dot network by describing the orbitals as discrete levels with energy ε_i in H_0. We include inter dot tunneling in H_t and Coulomb repulsion between electrons in the triple dot network in H_C. The

Hamiltonian is

$$H = H_0 + H_t + H_C. \tag{4.3}$$

The non-interacting part of the Hamiltonian, H_0 and H_t, is

$$H_0 = \sum_{i,\sigma} \varepsilon_{i\sigma} c^\dagger_{i\sigma} c_{i\sigma} \tag{4.4}$$

$$H_t = \sum_{\sigma} {\sum_{i\neq j}}' t_{ij} c^\dagger_{i\sigma} c_{j\sigma} \quad t_{ij} = t^*_{ji} \tag{4.5}$$

$$i, j = L, M, M+\Delta, R \quad \sigma = \uparrow, \downarrow,$$

where t_{ij} is the tunneling coefficient between level i and j, and the prime on the summation means that we should exclude terms where $i, j = M, M+\Delta$ because H_t describes inter dot tunneling. The Coulomb operator is

$$H_C = \frac{1}{2} \sum_{\sigma,\sigma'} \sum_{i,j,k,l} \langle k\sigma, l\sigma' \left| V(\vec{x} - \vec{x'}) \right| i\sigma, j\sigma' \rangle \, c^\dagger_{k\sigma} c^\dagger_{l\sigma'} c_{j\sigma'} c_{i\sigma}. \tag{4.6}$$

The matrix elements are

$$\langle k\sigma, l\sigma' \left| V(\vec{x} - \vec{x'}) \right| i\sigma, j\sigma' \rangle = \int \mathrm{d}x \int \mathrm{d}x' \psi^*_{k\sigma} \psi^*_{l\sigma'} V(\vec{x} - \vec{x'}) \psi_{i\sigma} \psi_{j\sigma'} \tag{4.7}$$

$$V(\vec{x} - \vec{x'}) = \frac{e^2}{4\pi\epsilon} \frac{1}{\left| \vec{x} - \vec{x'} \right|} \tag{4.8}$$

$$i, j, k, l = L, M, M+\Delta, R \quad \sigma = \uparrow, \downarrow$$

where $\vec{x}$ ($\vec{x'}$) is the coordinates of the (primed) electron, ψ_i is the wave function of orbital i, e is the electron charge, and ϵ is the permittivity.

Model of Individual Dots

In order to estimate values of the parameters in the Hamiltonian above, we make a specific model of the quantum dot system. The confining potential in an actual lateral dot, described in Sec. 2.2.1, has some complicated form, but we can reproduce the most significant features of the dot behavior in a simple model.

For this work, the most important feature of the confining potential is that it leads to a discrete, tunable spectrum. This is also characteristic for simple potentials from elementary quantum mechanics such as the one dimensional infinite well potential. As discussed in Sec. 2.2.1 and Sec. A.4, we can tune its spectrum by adding a constant energy to all levels in the well or by adjusting the width of the well and thus the level spacing. We therefore choose this potential to model the individual dots.

Parameters in the Hamiltonian for 1D Infinite Well Dots

In the infinite well model, the energies of the discrete levels ε_i in Eq. 4.3 are the eigenenergies of the infinite well, see Eq. A.11. For this specific purpose, we require that the level spacing and the charging energy are much smaller for the middle dot than for the outer dots. We can obtain this by increasing the width of the middle well, or the size of the middle dot.

The tunneling Hamiltonian between subsystems is a term that arises due to the finite overlap of wavefunctions from different subsystems.[11] In the infinite well model, the wavefunctions are zero outside the wells. In the actual confining potential, on the other hand, there will be overlaps, and gates are attached to control the size of the tunnel barrier as described in Sec. 2.2.1. So, we include a tunneling Hamiltonian to the model to account for this. We assume that the tunnel barrier is large, which leads to a small t, so we need only include direct tunneling between neighboring dots. For simplicity, we assume that all tunneling coefficients are equal. The tunneling Hamiltonian is then

$$H_t = \sum_{\sigma} t(c^\dagger_{L\sigma}c_{M\sigma} + c^\dagger_{L\sigma}c_{M+\Delta\sigma} + c^\dagger_{R\sigma}c_{M\sigma} + c^\dagger_{R\sigma}c_{M+\Delta\sigma}) + h.c. \tag{4.9}$$

We evaluate the matrix elements of the Coulomb operator in Eq. 4.7 for a simplified model of the Coulomb interaction. We approximate Eq. 4.8 with a delta function interaction such that

$$V(x - x') = U'\delta(x - x') \tag{4.10}$$

where U' is the interaction strength, and $\delta(x)$ is the Dirac delta function. This also allows us to evaluate the matrix elements analytically.

In the infinite well model, there is no overlap between wavefunctions localized on different dots, so we obtain non-zero matrix elements involving two electrons on the same dot only. Because we exclude states with two electrons on a single outer dot from the Hilbert space as discussed in Sec. 4.1.1, the only non-zero matrix elements are for states with two electrons on the middle dot.

Furthermore, from Paulis exclusion principle, or Eq. A.19, we see that elements with $\sigma = \sigma'$ **and** ($i = j$ or $k = l$) vanish. We evaluate the non-zero elements with Eq. 4.7 where $i, j, k, l = M, M + \Delta$. The wavefunctions ψ_M and $\psi_{M+\Delta}$ are given in Eq. A.10 with $n = 1, 2$. This leads to integrals of the form

$$\frac{4U'}{a^2}\int_0^a \mathrm{d}x \int_0^a \mathrm{d}x' \sin\left(\pi\frac{x}{a}\right)^n \sin\left(2\pi\frac{x}{a}\right)^m \delta(x - x') \sin\left(\pi\frac{x'}{a}\right)^{n'} \sin\left(2\pi\frac{x'}{a}\right)^{m'} \tag{4.11}$$

where $m + n = 2$, and $m' + n' = 2$. After evaluation of the delta function, we obtain

$$\frac{4U'}{a^2}\int_0^a \mathrm{d}x \sin\left(\pi\frac{x}{a}\right)^k \sin\left(2\pi\frac{x}{a}\right)^l = \begin{cases} 0 & \text{for } k,l \text{ odd} \\ U & \text{for } k = l = 2 \\ \frac{3U}{2} & \text{for } k = 4 \text{ or } l = 4, \end{cases} \tag{4.12}$$

where $k = n + n'$, $l = m + m'$, and $U = U'/a$. The Coulomb operator evaluated for the infinite well model with a delta function interaction is then

$$\begin{aligned} H_C =& \frac{3U}{2}\left(c^\dagger_{M\uparrow}c^\dagger_{M\downarrow}c_{M\downarrow}c_{M\uparrow} + c^\dagger_{M+\Delta\uparrow}c^\dagger_{M+\Delta\downarrow}c_{M+\Delta\downarrow}c_{M+\Delta\uparrow}\right) \\ &+U\sum_{\sigma\sigma'}\left(c^\dagger_{M\sigma}c^\dagger_{M+\Delta\sigma'}c_{M+\Delta\sigma'}c_{M\sigma} + c^\dagger_{M\sigma}c^\dagger_{M+\Delta\sigma'}c_{M\sigma'}c_{M+\Delta\sigma}\right. \\ &\left. + c^\dagger_{M\uparrow}c^\dagger_{M\downarrow}c_{M+\Delta\downarrow}c_{M+\Delta\uparrow} + c^\dagger_{M+\Delta\uparrow}c^\dagger_{M+\Delta\downarrow}c_{M\downarrow}c_{M\uparrow}\right). \end{aligned} \tag{4.13}$$

The fact that the four terms in the last parenthesis have a common prefactor is due to the delta function approximation of the Coulomb interaction. If we had used the $1/(x - x')$ dependence, we would have a result of the form

$$\begin{aligned} H'_C =& U_1 c^\dagger_{M\uparrow}c^\dagger_{M\downarrow}c_{M\downarrow}c_{M\uparrow} + U_2 c^\dagger_{M+\Delta\uparrow}c^\dagger_{M+\Delta\downarrow}c_{M+\Delta\downarrow}c_{M+\Delta\uparrow} \\ &+\sum_{\sigma\sigma'}\left[U_3 c^\dagger_{M\sigma}c^\dagger_{M+\Delta\sigma'}c_{M+\Delta\sigma'}c_{M\sigma} + U_4\left(c^\dagger_{M\sigma}c^\dagger_{M+\Delta\sigma'}c_{M\sigma'}c_{M+\Delta\sigma}\right.\right. \\ &\left.\left. + c^\dagger_{M\uparrow}c^\dagger_{M\downarrow}c_{M+\Delta\downarrow}c_{M+\Delta\uparrow} + c^\dagger_{M+\Delta\uparrow}c^\dagger_{M+\Delta\downarrow}c_{M\downarrow}c_{M\uparrow}\right)\right]. \end{aligned} \tag{4.14}$$

If we want to see an increase in the singlet population, it turns out to be extremely important that $U_3 \neq U_4$, as we will see later in Sec. 4.2.5. Therefore we modify the result obtained from the infinite well and delta function potential such that the Coulomb operator is

$$\begin{aligned} H_C =& \frac{3U}{2}\left(c^\dagger_{M\uparrow}c^\dagger_{M\downarrow}c_{M\downarrow}c_{M\uparrow} + c^\dagger_{M+\Delta\uparrow}c^\dagger_{M+\Delta\downarrow}c_{M+\Delta\downarrow}c_{M+\Delta\uparrow}\right) \\ &+\sum_{\sigma\sigma'} U c^\dagger_{M\sigma}c^\dagger_{M+\Delta\sigma'}c_{M+\Delta\sigma'}c_{M\sigma} + J\left(c^\dagger_{M\sigma}c^\dagger_{M+\Delta\sigma'}c_{M\sigma'}c_{M+\Delta\sigma}\right. \\ &\left. + c^\dagger_{M\uparrow}c^\dagger_{M\downarrow}c_{M+\Delta\downarrow}c_{M+\Delta\uparrow} + c^\dagger_{M+\Delta\uparrow}c^\dagger_{M+\Delta\downarrow}c_{M\downarrow}c_{M\uparrow}\right). \end{aligned} \tag{4.15}$$

In this way, we can vary U and J independently later. For the delta function interaction $U = J$, but it comes from the approximation, and later on we consider other models qualitatively where $J \neq U$. So we find it easiest to

keep them separate from the beginning. The symbols are short hand for the value of the following matrix elements

$$\begin{aligned}\frac{3}{2}U &= \langle M, M|V|M, M\rangle = \langle M+\Delta, M+\Delta|V|M+\Delta, M+\Delta\rangle \\ U &= \langle M, M+\Delta|V|M, M+\Delta\rangle = \langle M, M+\Delta|V|M+\Delta, M\rangle \\ J &= \langle M, M+\Delta|V|M+\Delta, M\rangle = \langle M+\Delta, M|V|M, M+\Delta\rangle \\ &= \langle M, M|V|M+\Delta, M+\Delta\rangle = \langle M+\Delta, M+\Delta|V|M, M\rangle\,. \end{aligned} \tag{4.16}$$

Exchange

We mentioned above that we want to employ a blockade phenomenon where 1001-triplet states leak out faster than 1001-singlets. This is possible if $J \neq U$, because the 1001-triplets can be tuned to be on resonance with the 0110-triplets without tuning the singlet states to be resonant. This effect is due to the exchange interaction.

With the Coulomb operator set in Eq. 4.15, we can see how this comes about. We calculate the expectation value of the Coulomb operator in the 0110-singlet and the 0110-triplet with $\chi = T_0$. In terms of second quantization operators, see Sec. A.6 the states are

$$|T_0\rangle = \frac{1}{\sqrt{2}}\left(c^\dagger_{M,\uparrow}c^\dagger_{M+\Delta,\downarrow} + c^\dagger_{M,\downarrow}c^\dagger_{M+\Delta,\uparrow}\right)|0\rangle \tag{4.17}$$

$$|S\rangle = \frac{1}{\sqrt{2}}\left(c^\dagger_{M,\uparrow}c^\dagger_{M+\Delta,\downarrow} - c^\dagger_{M,\downarrow}c^\dagger_{M+\Delta,\uparrow}\right)|0\rangle\,. \tag{4.18}$$

The expectation value for $|T_0\rangle$ is

$$\begin{aligned}\langle T_0|H_C|T_0\rangle &= \frac{1}{4}\sum_{\sigma,\sigma'}\sum_{a,b,c,d}\langle c\sigma, d\sigma'|V|a\sigma, b\sigma'\rangle \\ &\times \langle 0|\left(c_{M+\Delta,\downarrow}c_{M,\uparrow} + c_{M+\Delta,\uparrow}c_{M,\downarrow}\right)c^\dagger_{c\sigma}c^\dagger_{d\sigma'}c_{b\sigma'}c_{a\sigma}\left(c^\dagger_{M,\uparrow}c^\dagger_{M+\Delta,\downarrow} + c^\dagger_{M,\downarrow}c^\dagger_{M+\Delta,\uparrow}\right)|0\rangle \\ &= \langle M+\Delta, M|V|M+\Delta, M\rangle - \langle M, M+\Delta|V|M+\Delta, M\rangle = U - J \end{aligned} \tag{4.19}$$

The result for the 0110-triplet states does not depend on which triplet state we use, so we would get the same result for $\chi = T_+, T_-$. By an analogous calculation we find the expectation value of H_C for $|S\rangle$

$$\langle S|H_C|S\rangle = \langle M+\Delta, M|V|M+\Delta, M\rangle + \langle M, M+\Delta|V|M+\Delta, M\rangle = U + J \tag{4.20}$$

For the infinite well model with a delta function interaction, U is equal to J which leads to $\langle T_0|H_C|T_0\rangle = 0$ and $\langle S|H_C|S\rangle = 2U$.

We can understand why the Coulomb repulsion is larger for a singlet state than a triplet state using our knowledge on the spatial parts of the

states from Sec. 3.1.2. The expectation value of the distance between two indistinguishable particles with a spatially symmetric wavefunction is smaller than for an antisymmetric spatial wavefunction[24]. The singlet (triplet) has an (anti)symmetric spatial part and the Coulomb repulsion will thus be smaller for the triplet.

4.1.3 Role of the Reservoirs and Blockade in Transport Through the Triple Dot Network

With the Hamiltonian of the isolated triple dot network in place, we are ready to consider the effect of the incoming and outgoing rates. As described in Sec. 4.1, we assume that the bias window is such that only zero, one, and certain two-electron states are allowed in the network.

We choose γ_{in} to be large compared to γ_{out} such that when an electron leaks out of the network, a new one leaks in shortly after.

The coupling to the drain reservoir allows electrons to tunnel out of the network. This leakage is possible, because the coupling to the drain mixes the single particle states on the middle dot with the states in the drain. Due to the mixing, the discrete levels are no longer eigenstates to the
energy levels are broadened and their lifetimes become finite.[11]

We assume that states with 1 (2) electrons on the middle dot have a outgoing rate of (2)γ_{out} due to their coupling to the drain reservoir. In Fig. 4.2, we illustrate the different states on an energy scale for $t = 0$ and an otherwise unspecified configuration of parameters.

From Sec. 2.2.2, we know that coupling a dot network to a source and a drain reservoir may give rise to electron transport through the dot network if one or more electrochemical potential levels of the dot network are within the bias window. In our case, there are several levels within the bias window. However, transport through some states might be suppressed or blocked as it was the case for the triplet states in Pauli blockade described in Sec. 2.2.3.

We want to employ a new blockade phenomenon to enhance the steady state population of the 1001-singlet population. It is similar to Pauli blockade in the sense that the spin part of the state determines whether transport is blocked or not. It is different because in this scheme, the singlet state is blocked without the application of a magnetic field.

A perturbation, here the tunneling Hamiltonian from Eq. 4.9, mixes states that are close in energy more than states far apart, see Sec. A.5. We consider a tuning of the system such that the 1001-triplet states are on

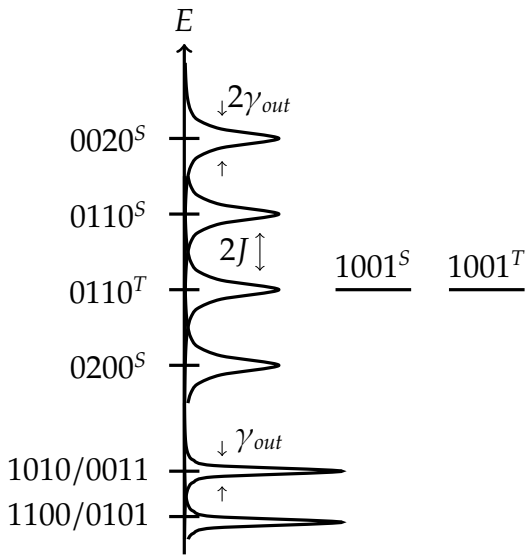

Figure 4.2: Energies of the states in the dot system for some parameter configuration. States with 1 (2) electrons on the middle dot are broadened proportionally to their outgoing rates (2)γ_{out}. The distance between the 0110-singlet and 0110-triplet states is $2J$. The 1001-states have the same energy due to the very small coupling between the two outer dots.

resonance with the 0110-triplets, while the 1001-singlet is off-resonance with the singlet states with both electrons on the middle dot, and while the 1001-states are off-resonant with all states with one electron on the middle dot. When tunneling is turned on, the two electrons in the 1001-triplets tunnel to the middle dot at a much higher rate than the two electrons in the 1001-singlet or one electron on its own. This way, the 1001-triplets may leak out much faster than the 1001-singlet. If this effect is significant, we say that the 1001-singlet is blocked.

The broadening of the levels on the middle dot is proportional to their outgoing rates. If γ_{out} gets too big compared to the spacing of states on the middle dot, they will overlap, and it will not be possible to tune the system such that only the 0110-triplets are resonant with the 1001-states. Therefore, we expect the blockade to decrease with increasing γ_{out}. The tunneling coupling t also broadens the energy levels, so it too should be small compared to the energy difference between the states of the system.

4.2 Perturbative treatment

In this section, we put the qualitative picture of the previous subsection onto more firm theoretical footing.

The 1001-states have an effective outgoing rate due to the tunneling coupling to the states on the middle dot. The effective outgoing rate of a 1001-state is larger if it is on resonance with a state with one or more electrons on the middle dot.

We use perturbation theory, see Sec. A.5, to estimate the effective outgoing rates of the 1001-singlet and triplet states respectively. We take the tunneling coefficient t to be small compared to the energy difference of any two states i and j that are directly coupled by H_t

$$t \ll \varepsilon_i - \varepsilon_j, \tag{4.21}$$

and use this as our perturbation parameter.

We estimate the effective outgoing rate of the 1001-states in the following way: First we find the first and second order corrections to the 1001-triplets and 1001-singlet, respectively, using Eq. A.12 and Eq. A.13. The corrections consist of states with one or more electrons on the middle dot. We estimate the effective outgoing rate of the initial state due to its mixing with state j as the absolute square of the coefficient c_j in the correction times the outgoing rate of state j, γ_j. Because the initial state might mix with more states with a non-zero outgoing rate, we sum over all contributions. The effective outgoing rate of a 1001-singlet γ^S_{out} or 1001-triplet state γ^T_{out} is thus given by

$$\gamma^{S/T}_{out} = \sum_j \left| c^{S/T}_j \right|^2 \gamma_{out_j}. \tag{4.22}$$

We take both first and second order corrections into account in the estimate in order to include two-electron tunneling events where the 1001-states couple to states with two electrons on the middle dot, so we capture the difference between singlet and triplet states.

We estimate the relative steady state population of the 1001-singlet and 1001-triplet states by taking the ratio of their effective outgoing rates

$$\eta = \gamma^T_{out}/4\gamma^S_{out}. \tag{4.23}$$

When the outgoing rate of the triplet states is larger than the outgoing rate of the singlet state, we expect a larger 1001-singlet population and $\eta > 1/4$. We introduce the factor of 4 because there are three 1001-triplet states and one 1001-singlet state, and we assume that the probability of an initial singlet and each of the triplet states are equal. If the outgoing rates are equal, we expect that the ratio of the steady state populations is 1/4.

4.2.1 Unperturbed Energies

We need the unperturbed energies in the following calculation, so we list them all here for convenience.

$$\begin{aligned}
E^0_{1001} &= \varepsilon_L + \varepsilon_R \\
E^0_{1100} &= \varepsilon_L + \varepsilon_M \\
E^0_{0101} &= \varepsilon_R + \varepsilon_M \\
E^0_{1010} &= \varepsilon_L + \varepsilon_M + \Delta \\
E^0_{0011} &= \varepsilon_M + \Delta + \varepsilon_R \\
E^0_{0200} &= 2\varepsilon_M + 3/2U \\
E^0_{0020} &= 2\varepsilon_M + 2\Delta + 3/2U \\
E^0_{0110T} &= 2\varepsilon_M + \Delta + U - J \\
E^0_{0110S} &= 2\varepsilon_M + \Delta + U + J
\end{aligned} \tag{4.24}$$

4.2.2 First Order Correction

To first order the initial 1001-state couples to states with one electron on the middle dot: $|1100\rangle, |1010\rangle, |0101\rangle,$ and $|0011\rangle$. The first order correction to the initial state is, by Eq. A.12

$$\begin{aligned}
|1001\rangle^1_\chi = &\frac{t}{E^0_{1001} - E^0_{1100}} |1100\rangle^0_\chi + \frac{t}{E^0_{1001} - E^0_{0101}} |0101\rangle^0_\chi \\
&+ \frac{t}{E^0_{1001} - E^0_{1010}} |1010\rangle^0_\chi + \frac{t}{E^0_{1001} - E^0_{0011}} |0011\rangle^0_\chi
\end{aligned} \tag{4.25}$$

$\chi = T_+, T_-, T_0, S$

where the subscript χ indicates that the expression is valid for all the four spin states. Superscript 0 indicates that it is an eigenstate or eigenenergy of the unperturbed Hamiltonian i.e. for $t = 0$, whereas superscipt 1 indicates that it is a first order correction.

Using Eq. 4.22, the contribution to the effective outgoing rate from the first order correction becomes

$$\begin{aligned}
\gamma^1_{out} = \gamma_{out} t^2 \Bigg[&\frac{1}{(E^0_{1001} - E^0_{1100})^2} + \frac{1}{(E^0_{1001} - E^0_{0101})^2} \\
&+ \frac{1}{(E^0_{1001} - E^0_{1010})^2} + \frac{1}{(E^0_{1001} - E^0_{0011})^2} \Bigg].
\end{aligned} \tag{4.26}$$

4.2.3 Second Order Correction to the 1001-Triplet State

The second order correction to initial triplet states is, by Eq. A.13

$$|1001\rangle_T^2 = \frac{t^2}{\left(E^0_{1001} - E^0_{0110T}\right)}\left[\frac{-1}{\left(E^0_{1001} - E^0_{1100}\right)} + \frac{1}{\left(E^0_{1001} - E^0_{1010}\right)} - \frac{1}{\left(E^0_{1001} - E^0_{0011}\right)} + \frac{1}{\left(E^0_{1001} - E^0_{0101}\right)}\right]|0110\rangle_T^0 \quad (4.27)$$

$T = T_+, T_-, T_0$.

The second order correction contributes with an effective outgoing rate of

$$\gamma_{out}^{2T} = \frac{2\gamma_{out}\cdot t^4}{\left(E^0_{1001} - E^0_{0110T}\right)^2}\left[\frac{-1}{\left(E^0_{1001} - E^0_{1100}\right)} + \frac{1}{\left(E^0_{1001} - E^0_{1010}\right)} - \frac{1}{\left(E^0_{1001} - E^0_{0011}\right)} + \frac{1}{\left(E^0_{1001} - E^0_{0101}\right)}\right]^2. \quad (4.28)$$

Note the minus signs in the square brackets. They create the possibility of destructive interference, which we return to in Sec. 4.2.5.

In Sec. 4.1.3, we emphasized that we expect the steady state 1001-singlet population to be large when the 0110- and 1001-triplets are resonant. We see that on the resonance $E^0_{1001} = E^0_{0110T}$, the expression in Eq. 4.28 blows up. It happens because the perturbative expression is not valid on the resonance or in its vicinity since it builds on the assumption $t \ll \varepsilon_i - \varepsilon_j$ in Eq. 4.21, which is not fulfilled. As a consequence, the value of the effective outgoing rates should not be trusted too close to a resonance. Though we cannot trust the value, we trust that if the effective outgoing rate diverges in the perturbative expression in certain points, the actual outgoing rate will increase on those points and in their vicinity.

4.2.4 Second Order Correction to the 1001-Singlet State

The second order correction to an initial singlet state is by Eq. A.13

$$\begin{aligned}|1001\rangle_S^2 =& \frac{t^2}{\left(E^0_{1001}-E^0_{0110S}\right)}\left[\frac{1}{\left(E^0_{1001}-E^0_{1100}\right)}+\frac{1}{\left(E^0_{1001}-E^0_{1010}\right)}\right.\\ &\left.+\frac{1}{\left(E^0_{1001}-E^0_{0011}\right)}+\frac{1}{\left(E^0_{1001}-E^0_{0101}\right)}\right]|0110\rangle^{S,0}\\ &+\frac{\sqrt{2}t^2}{\left(E^0_{1001}-E^0_{0200}\right)}\left[\frac{1}{\left(E^0_{1001}-E^0_{1100}\right)}+\frac{1}{\left(E^0_{1001}-E^0_{0101}\right)}\right]|0200\rangle^{S,0}\\ &+\frac{\sqrt{2}t^2}{\left(E^0_{1001}-E^0_{0020}\right)}\left[\frac{1}{\left(E^0_{1001}-E^0_{1010}\right)}+\frac{1}{\left(E^0_{1001}-E^0_{0011}\right)}\right]|0020\rangle^{S,0}.\end{aligned} \tag{4.29}$$

The second order correction to the singlet contributes with an effective outgoing rate of

$$\begin{aligned}\gamma^{S2}_{out} =& 2\gamma_{out}\cdot t^4\left(\frac{1}{\left(E^0_{1001}-E^0_{0110S}\right)^2}\left[\frac{1}{\left(E^0_{1001}-E^0_{1100}\right)}+\frac{1}{\left(E^0_{1001}-E^0_{1010}\right)}\right.\right.\\ &\left.+\frac{1}{\left(E^0_{1001}-E^0_{0011}\right)}+\frac{1}{\left(E^0_{1001}-E^0_{0101}\right)}\right]^2\\ &+\frac{2}{\left(E^0_{1001}-E^0_{0200}\right)^2}\left[\frac{1}{\left(E^0_{1001}-E^0_{1100}\right)}+\frac{1}{\left(E^0_{1001}-E^0_{0101}\right)}\right]^2\\ &\left.+\frac{2}{\left(E^0_{1001}-E^0_{0020}\right)^2}\left[\frac{1}{\left(E^0_{1001}-E^0_{1010}\right)}+\frac{1}{\left(E^0_{1001}-E^0_{0011}\right)}\right]^2\right)\end{aligned} \tag{4.30}$$

4.2.5 Analysis of the Ratio of Outgoing Rates

We combine the results of the last subsection to the final expression of η

$$\eta = \frac{\gamma^1_{out}+\gamma^{T2}_{out}}{4(\gamma^1_{out}+\gamma^{S2}_{out})}. \tag{4.31}$$

We expect to see η increase or decrease significantly for parameters where either of the 0110-triplet states, the 0110-singlet, 0200-singlet, and 0020-singlet states are resonant with the 1001-states. We do not expect significant changes in η for resonances of the 1001-states and states with only one electron on the middle dot, because they enter both the numerator and the denominator.

However, it is not necessarily the case that η changes significantly on these resonances. As mentioned in Sec. 4.2.3 there are two minus signs in Eq. 4.28 that may give rise to destructive interference. To see this, we simplify Eq. 4.28 using the energies in terms of the parameters of the triple dot network listed in Eq. 4.24:

$$\begin{aligned}\gamma_{out}^{T2} =& \frac{2 \cdot \gamma_{out} t^4}{(\varepsilon_L + \varepsilon_R - 2\varepsilon_M - \Delta - U + J)^2} \\ &\times \left[\frac{\Delta(\varepsilon_R - \varepsilon_L)(\Delta + 2\varepsilon_M - \varepsilon_L - \varepsilon_R)}{(\varepsilon_L - \varepsilon_M)(\varepsilon_L - \varepsilon_M - \Delta)(\varepsilon_R - \varepsilon_M)(\varepsilon_R - \varepsilon_M - \Delta)} \right]^2 . \end{aligned} \tag{4.32}$$

On the 1001-triplet and 0110-triplet resonance, the level spacing on the middle dot can be expressed in terms of the other parameter of the triple dot

$$\Delta \overset{\text{res.}}{=} \varepsilon_R + \varepsilon_L - 2\varepsilon_M - U + J. \tag{4.33}$$

We substitute this value of Δ into the small parenthesis in the numerator of the rightmost fraction in a square bracket.

$$\begin{aligned}\gamma_{out}^{T2} =& \frac{2 \cdot \gamma_{out} t^4}{(\varepsilon_L + \varepsilon_R - 2\varepsilon_M - \Delta - U + J)^2} \\ &\times \left[\frac{\Delta(\varepsilon_R - \varepsilon_L)(J - U)}{(\varepsilon_L - \varepsilon_M)(\varepsilon_L - \varepsilon_M - \Delta)(\varepsilon_R - \varepsilon_M)(\varepsilon_R - \varepsilon_M - \Delta)} \right]^2 \end{aligned} \tag{4.34}$$

The perturbative estimate of γ_{out}^{T2} diverges when the denominator of the left fraction, outside the square bracket, goes to zero, $\varepsilon_L + \varepsilon_R - 2\varepsilon_M - \Delta - U + J \to 0$, unless either of the equations

$$\Delta = 0, \quad \varepsilon_L = \varepsilon_R, \quad U = J, \tag{4.35}$$

are fulfilled. If one or more of these conditions are fulfilled, the numerator of the rightmost fraction, in square brackets, is zero, canceling the zero in the denominator of the leftmost fraction. We do not expect to see an increase in the effective outgoing rate of the 1001-triplet state, and thereby the steady state 1001-singlet population, for parameters close to, or actually fulfilling, one or more of these conditions.

4.3 Comparison of the Perturbative Treatment and the Steady State of the Master Equation

In this section, we describe how we set up the master equation of the triple dot network and compare with the results of the perturbative treatment above.

We use the numerical tool described in Sec. 3.4 to set up the master equation for the triple dot system and to find its steady state solutions. For $\Delta = 0$ we use both versions of the numerical tool: a) for which the two degenerate levels are assumed to couple to two different reservoirs and b) where they couple to the same reservoir. We find steady state population of a given state by defining the projection operator of the state and tracing over the steady state density operator and the projection operator according to Eq. 3.3.

To get an overview of how well the perturbative treatment and the steady state solution of the master equation agree, we want to plot the perturbative estimate of the steady state 1001-singlet population η and the steady 1001-singlet population found with the master equation S_p as functions of the middle dot parameters ε_M and Δ.

We expect that η and S_p deviate from 1/4 when either of the states with two electrons on the middle dot listed in Eq. 4.24 are on resonance with the 1001-states. We choose to vary the energy levels on the outer dots such that $\varepsilon_L = -\varepsilon_R$. For this choice, the energies of the 1001-states are always zero, so the resonance statement is equivalent to requiring that the energy levels in Eq. 4.24 equal zero. Thus we expect to see features for

$$\begin{aligned} E_{0200} &: \varepsilon_M = -3/4U \\ E_{0020} &: \Delta = -\varepsilon_M - 3/4U \\ E_{0110^T} &: \Delta = -2\varepsilon_M - U + J \\ E_{0110^S} &: \Delta = -2\varepsilon_M - (U + J). \end{aligned} \tag{4.36}$$

We make a specific choice of parameters: $U/\gamma_{in} = 8$, $J/\gamma_{in} = U/(4\gamma_{in})$, $\varepsilon_R/\gamma_{in} = -\varepsilon_L/\gamma_{in} = 1$ and $t/\gamma_{in} = \gamma_{out}/\gamma_{in} = 0.005$. In the following all parameters are expressed relative to γ_{in}. We indicate that a parameter is relative to γ_{in} with a bar, e.g. $\bar{t} = t/\gamma_{in}$. For this choice of parameters, we expect lines at

$$\begin{aligned} E_{0200} &: \bar{\varepsilon}_M = -6 \\ E_{0020} &: \bar{\Delta} = -\bar{\varepsilon}_M - 6 \\ E_{0110^T} &: \bar{\Delta} = -2\bar{\varepsilon}_M - 6 \end{aligned}$$

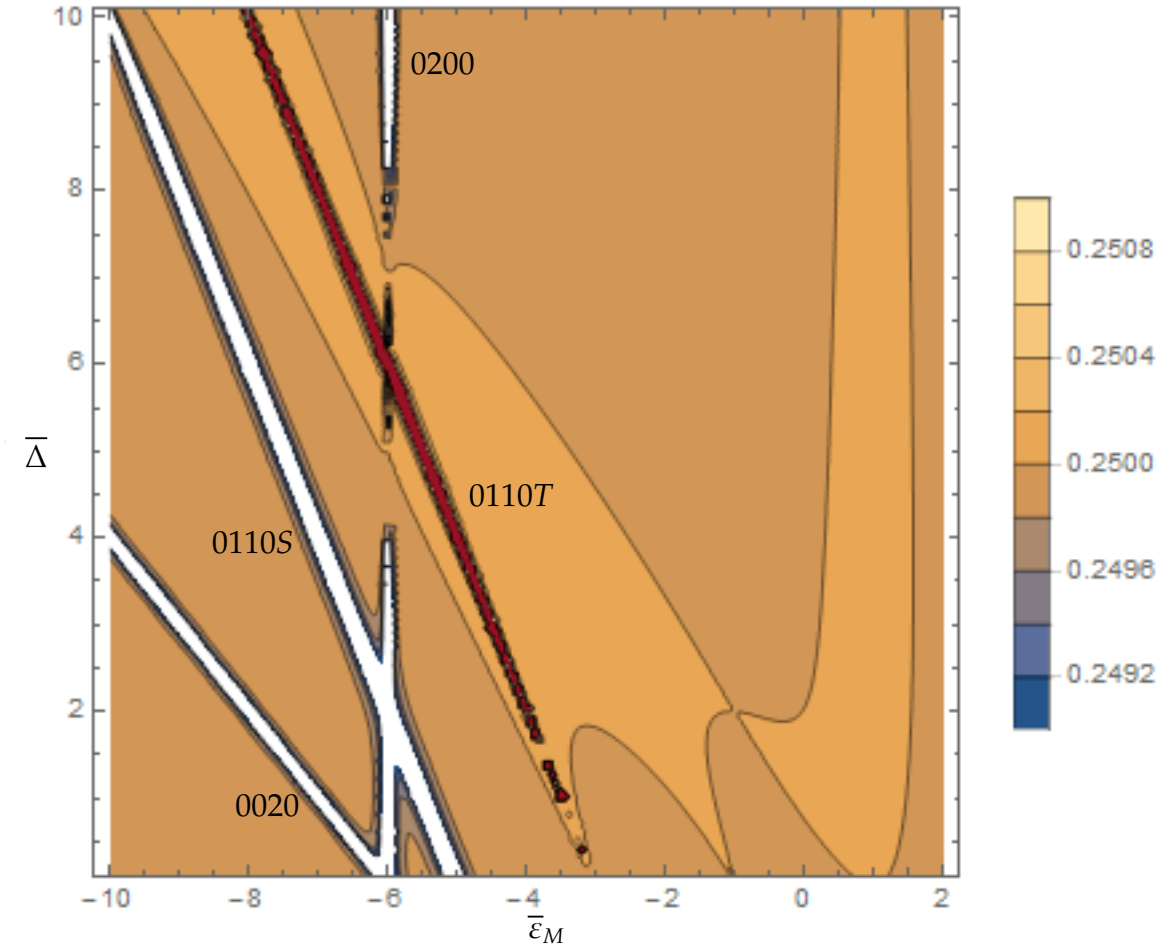

Figure 4.3: Contour plot of the perturbative estimate of the steady state 0110-singlet population. We plot the perturbative estimate of the steady state population of the 1001-singlet η as a function of energy of the lowest level on the middle dot $\overline{\varepsilon}_M \in [-10, 2]$ and level spacing on the middle dot $\overline{\Delta} \in [0.1, 10.1]$. White areas correspond to $\eta < 0.249$ and red areas correspond to $\eta > 0.251$. Values of $\eta \in [0.249, 0.251]$ are colored according to the color bar.

$$E_{0110^S} : \overline{\Delta} = -2\overline{\varepsilon}_M - 10. \tag{4.37}$$

We plot η as function of $\overline{\varepsilon}_M$ and $\overline{\Delta}$ in Fig. 4.3. We see the four expected lines in the plot and that η is very close to constant for all other parameters.

We make a corresponding plot of the steady state 1001-singlet population from the master equation in Fig. 4.4. We see that the expected lines are present although the line corresponding to the 0200-state being on resonance with the 1001-states is weak. There are four more lines, which

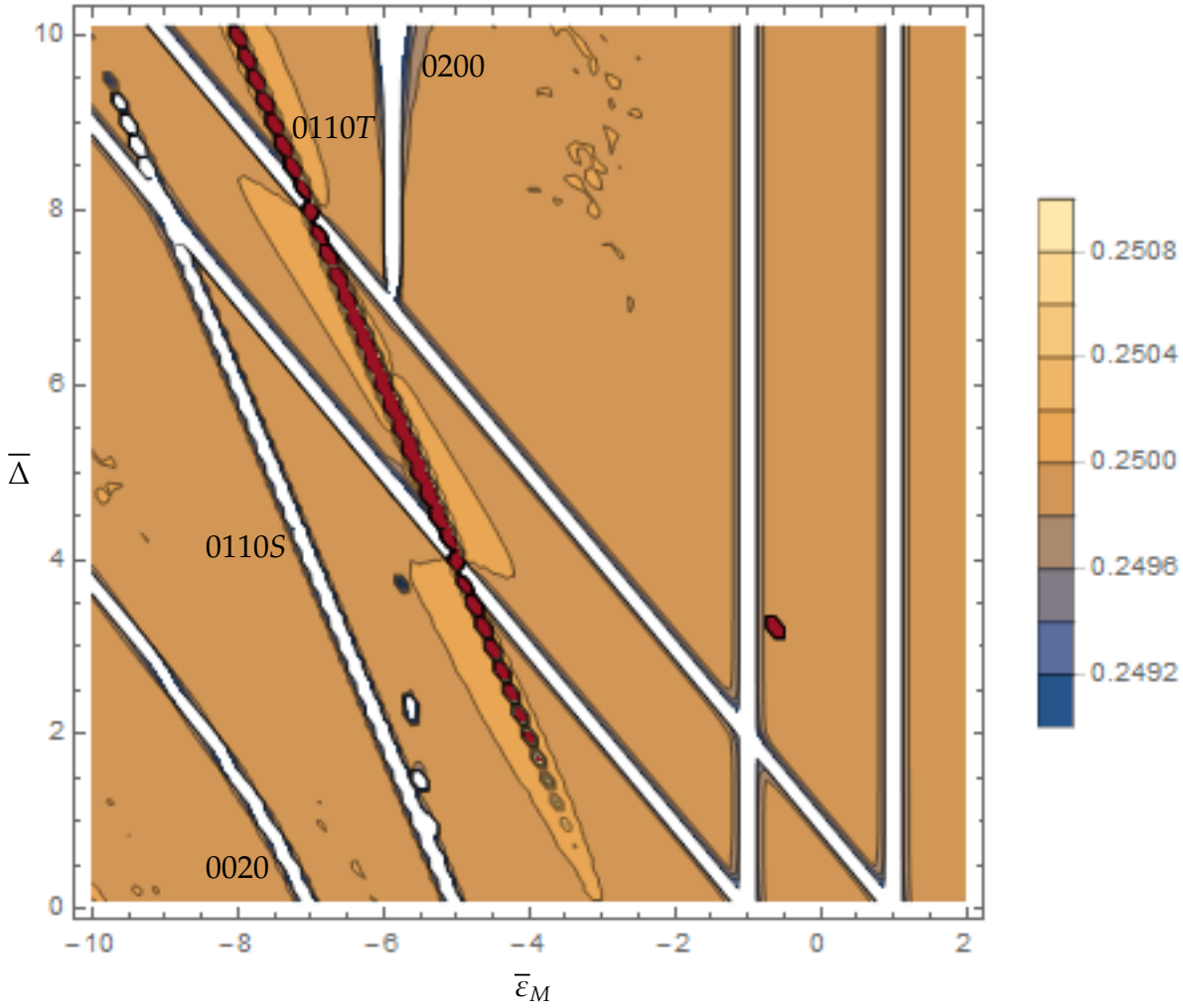

Figure 4.4: Contour plot of the steady state 1001-singlet population. We plot the steady state population of the 1001-singlet S_p as a function of the energy of the lowest level on the middle dot $\overline{\varepsilon}_M \in [-10, 2]$ and level spacing on the middle dot $\overline{\Delta} \in [0.1, 10.1]$. White areas correspond to $S_p < 0.249$ and red areas correspond to $S_p > 0.251$. Values of $S_p \in [0.249, 0.251]$ are colored according to the color bar.

correspond to resonances of states with one electron on the middle dot and the 1001-states. We return to these lines below in the comments on Fig. 4.6. As in Fig. 4.3, we see that the singlet population is very close to constant for all other parameters.

Comparing Fig. 4.3 and Fig. 4.4, the placement of the features due to the resonances of the 0200-singlet, 0020-singlet, 0110-singlet and the 0110-triplets in the contourplot of η and S_p appear be in good accordance. To see this more clearly and to see how the steady state singlet population

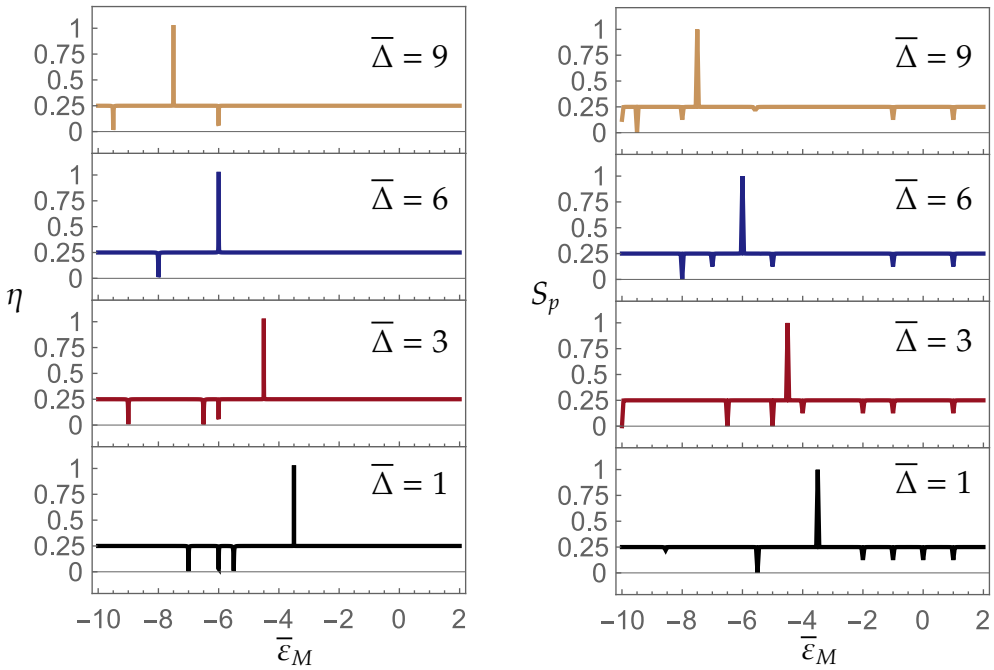

((a)) Perturb. estimate **((b))** Master Equation

Figure 4.5: Linecuts through Fig. 4.3 in a) and Fig. 4.4 in b). We plot the the perturbative estimate of η and the steady state 0110-singlet population S_p as functions of the energy of the lowest level on the middle dot $\overline{\varepsilon}_M$ for level spacing on the middle dot $\overline{\Delta} = 1, 3, 6, 9$. In the top panel, $\overline{\Delta} = 9$ and $\overline{\Delta} = 1$ in the bottom panel. We limit the plot range to $\eta \in [0, 1.0]$. The other parameters are $\overline{U} = 8$, $\overline{J} = \overline{U}/4$, $\overline{\varepsilon}_R = -\overline{\varepsilon}_L = 1$, and $\gamma_{out} = t = 0.005$. We vary $\overline{\varepsilon}_M$ in steps of 0.05.

varies in more detail, we make line cuts through the contour plots for $\overline{\Delta} = 1, 3, 6, 9$. We plot the linecuts in Fig. 4.5. We see that the steady state 1001-singlet population approaches 1 one the 1001-triplet and 0110-triplet resonance. The dips to zero are due to resonances between the 1001-singlet state with singlet states with two electrons on the middle dot. The minor dips are due to resonance of the 1001-states and states with one electron on the middle dot.

In Fig. 4.6, we plot the steady state poulation of the 1001-singlet, the 1001-triplets, and all 1001-states. We see that the total 1001-population is very close to 1 everywhere except for parameters where one of the states with one electron on the middle dot are resonant with the 1001-states. In those cases, it drops to being very close to 1/2. Otherwise, a dip in the 1001-singlet population corresponds to a peak in the 1001-triplet population and vice versa.

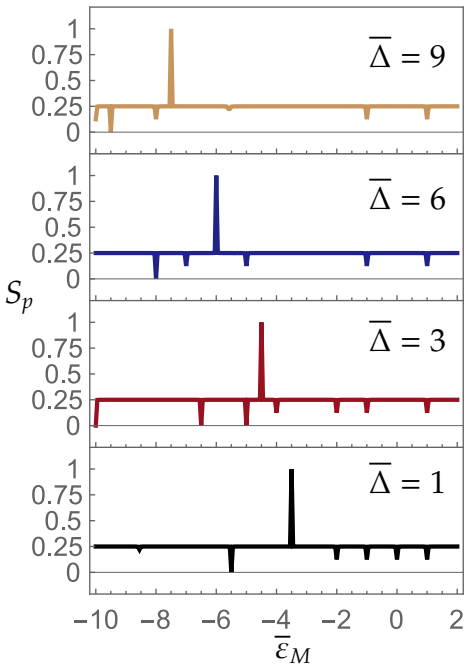

((a)) 1001-singlet Population

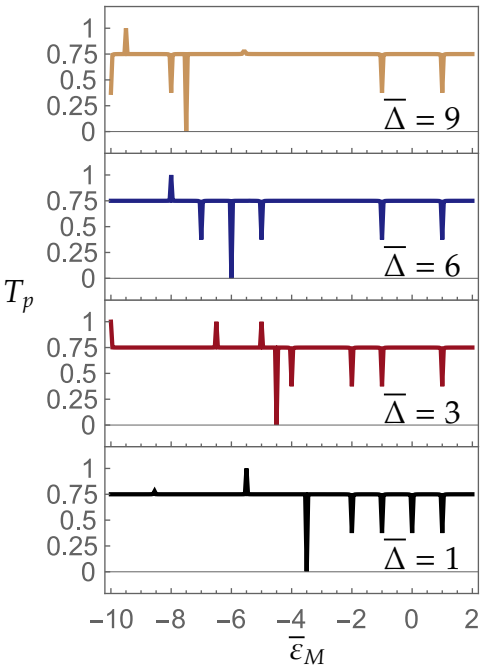

((b)) 1001-triplet Population

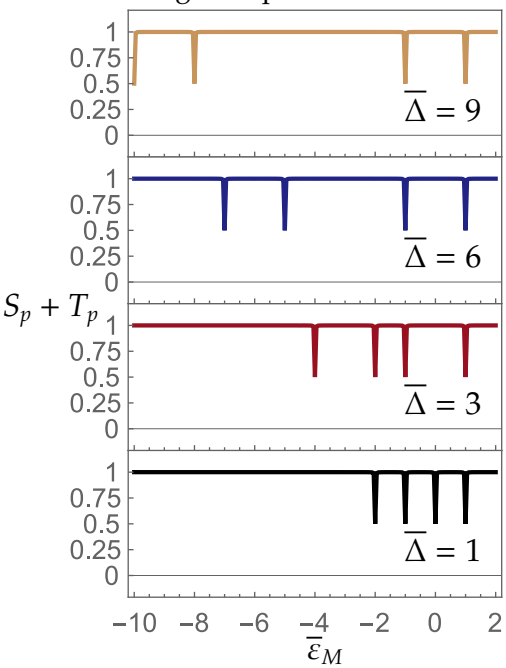

((c)) Total 1001-states Population

Figure 4.6: Populations in the steady state solution to the master equation as a function of the energy of the lowest level on the middle dot $\overline{\varepsilon}_M$ for three values of the detuning on the middle dot $\overline{\Delta} = 1, 3, 6, 9$. In a) we plot the 1001-singlet population S_p, in b) the 1001-triplet population T_p, and in c) the total population of 1001-states $S_p + T_p$. The other parameters are $\overline{U} = 8$, $\overline{J} = \overline{U}/4$, $\overline{\varepsilon}_R = -\overline{\varepsilon}_L = 1$, and $\overline{\gamma}_{out} = \overline{t} = 0.005$. We vary $\overline{\varepsilon}_M$ in steps of 0.05.

The results look promising. However, we need to make a small comment about the output of the code: Unfortunately, the steady state density operators calculated using the numerical tool are not perfectly Hermitian. As a consequence, the steady state singlet populations are complex numbers. However, we calculate the ratio of the imaginary and real part for all points used to make Fig. 4.5 b), Fig. 4.9 a) to d), and Fig. 4.10 a) and b). The largest absolute value of the ratio is of the order 10^{-5}, the mean is of the order 10^{-7}, and the median is of the order 10^{-8}. In total we include 3388 points. We suspect that the imaginary parts are due to some numerical error and that the real parts can be trusted. In all figures, we plot the real part of the populations.

In the Fig. 4.4, $\overline{\Delta} = 0$ is omitted, because the numerical tool is set up in such a way that we need to manually distinguish between situation a) where two or more degenerate levels couple to different reservoirs and situation b) where they couple to the same reservoir for the entire parameter range. However, version b) for $\overline{\Delta} = 0$ gives two steady states in all points on the line $\overline{\varepsilon}_M \in [-10, 2]$. We suspect that the situation is similar to the two levels coupled to a drain described in Sec. 3.3.2. Unfortunately, the resulting density operators are far from Hermitian. As an example, they can have diagonal elements with imaginary parts that are only one order of magnitude smaller than the real parts. Furthermore, some of the diagonal elements are negative. We believe it is because the direct outputs of the code $\rho^{\text{code}}_{ss,1}$ and $\rho^{\text{code}}_{ss,2}$ are linear combinations of the actual steady states of the system ρ^1_{ss} and ρ^2_{ss} with complex coefficients such that

$$\rho^{\text{code}}_{ss,1} = c_{11}\rho^1_{ss} + c_{12}\rho^2_{ss} \tag{4.38}$$

$$\rho^{\text{code}}_{ss,2} = c_{21}\rho^1_{ss} + c_{22}\rho^2_{ss}. \tag{4.39}$$

In principle, it should be possible to use our understanding of the two degenerate levels coupled to a drain from Sec. 3.3.2 to infer the coefficients and thus the actual steady state solutions. However, we find it more important for the time being to investigate the parameter dependence of the steady state 1001-singlet population for the non-degenerate case, and we thus leave this interesting question for further work.

In Fig. 4.7, we plot the steady state 1001-singlet population for $\overline{\Delta} = 0$ using version a) of the code. Physically, it corresponds to assuming that the two orbitals on the middle dot couple to two different reservoirs. We see that as expected from Eq. 4.34 there is no peak in the singlet population. In conclusion, the perturbative estimate is good for predicting the placement of features due to resonances of the 1001-states with states that have two electrons on the middle dot in the non-degenerate case.

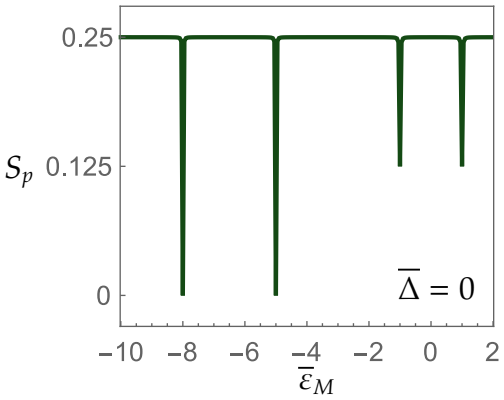

Figure 4.7: The steady state 1001-population S_p as a function of the energy of the levels on the middle dot $\overline{\varepsilon}_M$ for degenerate levels, ie $\overline{\Delta} = 0$. We plot the 1001-singlet population S_p as a function of the energy of $\overline{\varepsilon}_M$ for $\overline{\Delta} = 0$. The other parameters are $\overline{U} = 8$, $\overline{J} = \overline{U}/4$, $\overline{\varepsilon}_R = -\overline{\varepsilon}_L = 1$, $\overline{\gamma_{out}} = \overline{t} = 0.005$. We vary $\overline{\varepsilon}_M$ in steps of 0.05.

In Fig. 4.8, we zoom in on the singlet peaks in Fig. 4.5 to see the shape of the peaks for our initial choice of parameters. The figure serves as a reference for the following figures. From here, we investigate how the height and width of the peak are affected by the tunneling coefficient $\overline{t}$ and the misalignment of the energy levels on the outer dots $\overline{\varepsilon}_R = -\overline{\varepsilon}_L$. We investigate the dependence of the height and width on the incoming and outgoing rates, and the ratio $\overline{J}/\overline{U}$ in App. B and App. C.

In Fig. 4.9, we see that when we increase the tunneling coupling t, the height of the peak decreases and the width increase. We can understand the increase in width in the following way: Increasing t relaxes the resonance condition for the 1001-triplet and 0110-triplet states. On the other hand it also relaxes the resonance conditions for all other states and the 1001-singlet population and thereby the peak height decreases. This is in full accordance with our expectations from Sec. 4.1.3.

In Fig. 4.10 a) we see that when we decrease the misalignment of the outer dots, the width and height of the peak decrease as well. When the levels are aligned, $\overline{\varepsilon}_L = \overline{\varepsilon}_R = 0$, there is no peak in the singlet population as we predicted in Eq. 4.34. In Fig. 4.10 b) we see that the peak width does not depend monotonically on the misalignment. It first increases and then decreases. It would be very interesting to look into an optimal misalignment in future work. Increasing the misaligment to large values, we expect from Eq. 4.34 that the singlet population peak will decrease as the fraction in the parenthesis goes to zero when $|\overline{\varepsilon}_R| = |\overline{\varepsilon}_R| \to \infty$. In Fig. 4.10 c) and d) we see the peak height as a function of $\overline{\varepsilon}_R$. The over all trend is that it decreases with $\overline{\varepsilon}_R$. The decrease becomes significant for $\overline{\varepsilon}_R > \overline{\varepsilon}'_R$ where $\overline{\varepsilon}'_R \approx 10$. There are steep dips in the population when $\overline{\varepsilon}_R = -\overline{\varepsilon}_M$ and $\overline{\varepsilon}_R = -(\overline{\varepsilon}_M + \overline{\Delta})$ which correspond to the resonances of the states with one electron on the middle dot.

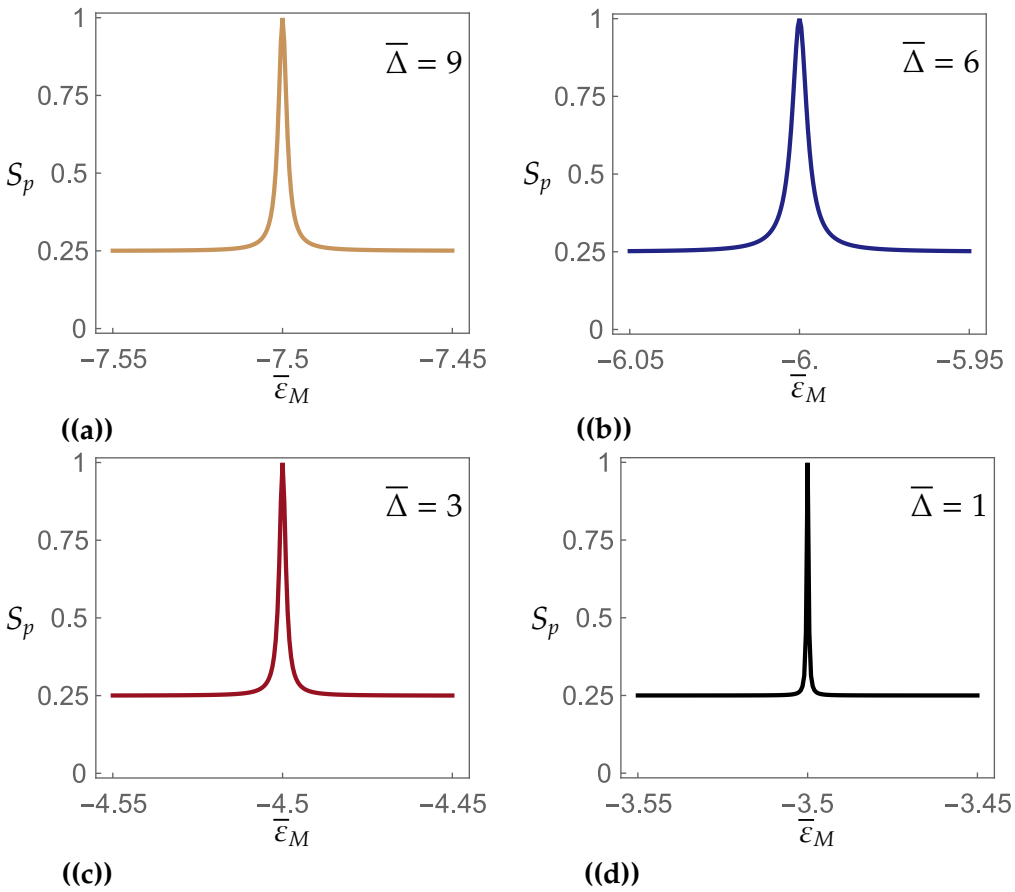

Figure 4.8: Zoom in on the peaks in the singlet populations on Fig. 4.5 b) to see the shape of the peaks. We plot the singlet population S_p as a function of the energy of the lowest single particle level on the middle dot $\overline{\varepsilon}_M$ for the level spacing on the middle dot $\overline{\Delta} = 9, 6, 3, 1$. The other parameters are $\overline{U} = 8$, $\overline{J} = \overline{U}/4$, $\overline{\varepsilon}_R = -\overline{\varepsilon}_L = 1$, and $\overline{\gamma}_{out} = \overline{t} = 0.005$. We vary $\overline{\varepsilon}_M$ in steps of $5 \cdot 10^{-4}$.

For the parameters investigated, the perturbative approach and the steady state 1001-singlet population are in good accordance with respect to the features due to the resonances of states with two electrons on the middle dot and the 1001-states. The steady state 1001-singlet population also shows features due to the resonances of states with one electron on the middle dot and the 1001-states. We understand how the peak height and width of the 1001-singlet population depend on the tunneling coupling t and the misalignment of the outer dots.

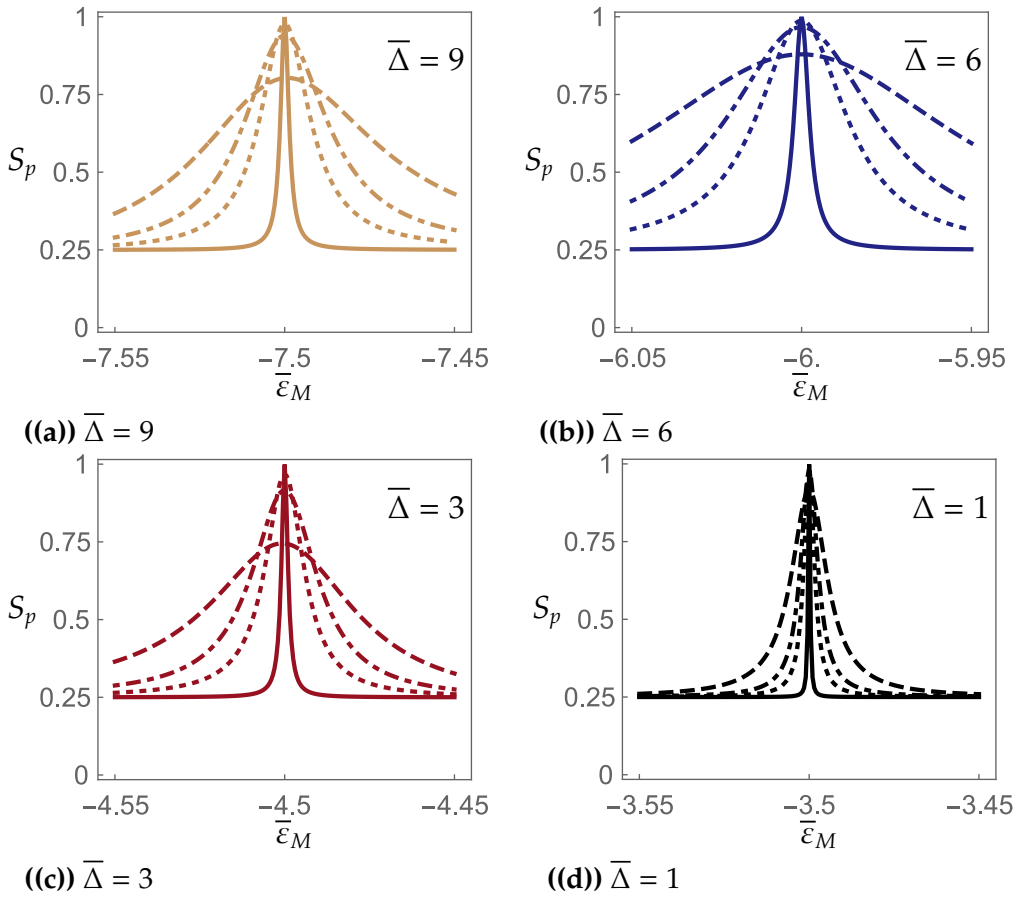

((a)) $\overline{\Delta} = 9$ **((b))** $\overline{\Delta} = 6$

((c)) $\overline{\Delta} = 3$ **((d))** $\overline{\Delta} = 1$

Figure 4.9: Singlet population peaks for different tunneling coefficients t. The four insets are the peaks in singlet population from Fig. 4.8 as a function of energy of the lowest level on the middle dot for level spacing $\overline{\Delta} = 1, 3, 6, 9$ for different tunneling couplings $\bar{t}$. The full lines is for $t = 0.005$, the dotted line for $\bar{t} = 0.03$, the dotdashed line for $\bar{t} = 0.05$, and the dashed line for $\bar{t} = 0.1$. The other parameters are $\overline{U} = 8$, $\overline{J} = 2$, and $\bar{t} = 0.005$. We vary $\overline{\varepsilon}_M$ in steps of $5 \cdot 10^{-4}$.

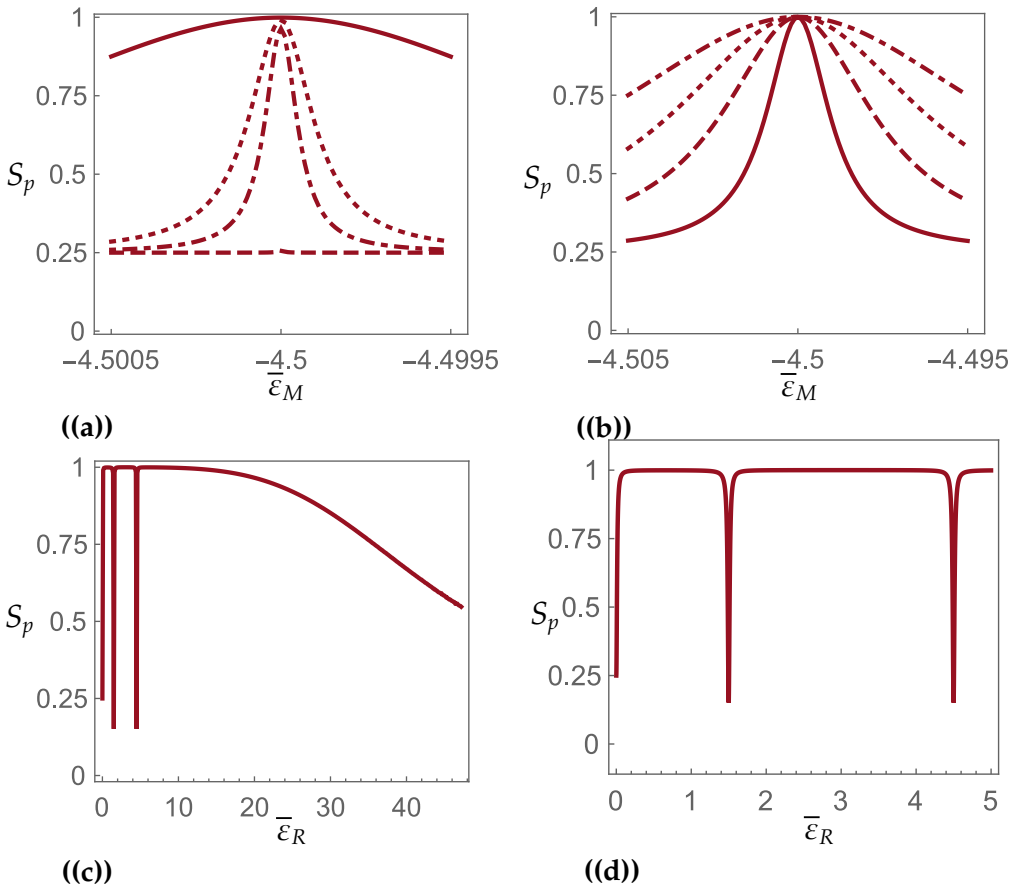

Figure 4.10: Singlet population peaks for different misalignments of the outer dots for $\overline{\Delta} = 3$. In a) and b) we plot the steady state 1001-singlet population as a function of the energy of the lowest single particle level on the middle dot $\overline{\varepsilon}_M$ for different values of energy levels on the outer dots under the constraint $\overline{\varepsilon}_R = -\overline{\varepsilon}_L$. In a) we decrease the value of the misalignment from $\overline{\varepsilon}_R = 1$ on the full line to $\overline{\varepsilon}_R = 0.1$ on the dotted line, $\overline{\varepsilon}_R = 0.05$ on the dotdashed line and finally $\overline{\varepsilon}_R = 0.001$ on the dashed line. In b) we increase the value of the misalignment from $\overline{\varepsilon}_R = 1$ on the full line to $\overline{\varepsilon}_R = 2.5$ on the dotted line, $\overline{\varepsilon}_R = 3$ on the dotdashed line and finally $\overline{\varepsilon}_R = 4$ on the dashed line. In c) we plot the peak height at $\overline{\varepsilon}_M = -4.5$ as a function of $\overline{\varepsilon}_R$. For $\overline{\varepsilon}_R > 47$, we obtain multiple steady state solutions. In d) we zoom in on the dips corresponding to $\overline{\varepsilon}_R = \overline{\varepsilon}_M$ and $\overline{\varepsilon}_R = \overline{\varepsilon}_M + \overline{\Delta}$ in the singlet population in c). The other parameters are $\overline{\Delta} = 3$, $\overline{U} = 8$, $\overline{J} = \overline{U}/4$, $\overline{\varepsilon}_R = -\overline{\varepsilon}_L = 1$ and $\overline{\gamma}_{out} = \overline{t} = 0.005$. We vary $\overline{\varepsilon}_M$ in steps of $5 \cdot 10^{-4}$.

4.4 Summary

In this chapter, we worked with a linear triple dot network with two small outer dots and a bigger middle dot. We investigated whether we could tune its parameters and coupling to the reservoirs such that the steady state of the system has a large population of the 1001-singlet state.

To do this, we first set up a Hamiltonian of the system that takes nearest neighbor tunneling between the dots and Coulomb repulsion on the middle dot explicitly into account. We modeled each dot as an infinite well to estimate the parameters in the Hamiltonian.

We used a perturbative approach to estimate the steady state 1001-singlet population where we assumed that the tunneling coefficient t is small compared to all level spacings in the spectrum and used it as the small parameter. We estimated the steady state population of the 1001-singlet state by taking the ratio of the effective outgoing rates of the 1001-singlet and 1001-triplet states. We used the first and second order corrections to the 1001-states to estimate their outgoing rates.

We also found the steady state population of the 1001-singlet from the master equation of the triple dot network. In the non-degenerate case we found that deviations from 1/4 in the perturbative estimate and the steady state population of the 1001-state due to resonances between the 1001-states and states with two electrons on the middle dot are in good accordance. Furthermore, from the perturbative approach we saw that we should not expected an increase in the 1001-singlet population if the energy levels on the outer dots are aligned $\overline{\varepsilon}_L = \overline{\varepsilon}_R$, the levels on the middle dot are aligned $\overline{\Delta}$.

The steady state 1001-singlet population approaches 1 when the 1001-triplets and 0110-triplets are resonant. The height and the width of the peak in population depends strongly on the tunneling coefficient $\bar{t}$ and misalignment of the energy levels on the outer dots as predicted from the perturbative approach.

CHAPTER 5

Discussion and Further Work

Our results suggest that it is possible to tune the parameters of the triple dot network and engineer its coupling to the environment such that the steady state population of the 1001-singlet approaches 1. However, before concluding there are certain issues related to the used approximations inherent in our work that should be discussed.

Our work is based on the assumption that we have tuned the parameters of the triple dot such that we may regard the electrochemical potential of the source as infinitely large compared to the electrochemical potentials of the included states of the dot network and infinitely small compared to the electrochemical potentials of the excluded states. Is such a regime realizable under realistic physical conditions? How are the results modified if additional states are included? These are important questions, which should be investigated in more detail in future work.

Additionally, we have discovered an issue with the numerical tool used to find the steady state solutions to the master equation: in some cases it returns steady state density matrices with small non-Hermitian components. However, due to the small relative size of the imaginary parts of the populations and the good accordance with our perturbative approach, we attribute the imaginary parts to numerical errors. If it is relevant to sort it out in future, we suggest the following two approaches to solve the non-Hermitian density operator problem: First and foremost, we could investigate the parameter space further to exclude that it is due to the relative sizes of the parameters in the region of parameter space that we have investigated so far. If it is not the case, we could change the method to find the steady state. One suggestion could be to continue

finding the steady states from the null space of $\underline{\underline{L}}$, but to rewrite the routine in such a way that the solution has to be expanded in a basis of Hermitian matrices with real coefficients. A completely different way is to solve the master equation with numerical integration from some initial state until the steady state is achieved.

Additionally, our model of the quantum dots might be too simple. The treatment of the overlap of wave functions localized on different dots, which is present in the actual confining potential but not in the infinite well model, is somewhat inconsistent. When we discuss the Coulomb repulsion we use the fact that the overlap is not present in the infinite well model to ignore terms in the Coulomb operator, but when we discuss tunneling coupling of the dots we argue that the overlap has to be there and put it in by hand. If we changed the dot model to harmonic oscillator potentials, the overlap would arise naturally in the model, and we would not compromise the simplicity of the model much. We have not done it yet due to limited time.

The delta function approximation of the Coulomb repulsion might also be too simple. It implies a relation J = U, which is not realistic, and gives rise to a situation in which the desired blockade effect is compromised. A different approximation that still allows for an analytical solution to the integrals should be chosen, or the integrals should be calculated numerically in stead with a more realistic model of the Coulomb repulsion. Furthermore, it might be relevant to include the Coulomb repulsion between electrons on different dots.

Chapter 6

Summary and Conclusions

The aim was to investigate whether it is possible to tune the parameters of a triple dot network and its coupling to reservoirs such that the steady state of the triple dot under transport has a large population of the singlet state with one electron on each of the outer dots. Though there are open questions remaining for future work, our results show that it is possible to achieve a population close to 1 for a range of parameters.

Our system is a linear triple dot network with small outer dots and a bigger middle dot. We assume that the bias window is such that all states of the network with three or more electrons are unaccessible, and that only the low energy orbitals of the dots can be occupied. More specifically, we assume that only the two lowest energy orbitals on the middle dot can be occupied, and that there cannot be more than one electron on each of the outer dots, which can only be in the ground state. The outer dots are coupled to source reservoirs, and the middle dot is coupled to a drain reservoir.

The main ingredient for achieving the large singlet population on the outer dots is the exchange splitting between the spin singlet and triplet states occupying two orbitals on the middle dot. We used this splitting to form a blockade phenomenon in transport through the dot network similar to Pauli blockade in the sense that some spin states are blocked and others are not.

We set up a model of the triple dot network where the individual dots are described by infinite well potentials, but electrons are allowed to tunnel between them. We take Coulomb repulsion between electrons on the same dot into account and model the Coulomb repulsion as a delta

function interaction.

We estimate the steady state populations in the dot network using a perturbative approach and by finding the steady state of the system's master equation derived under the Born and Markov approximations. From the perturbative approach we find that we expect an increase in the 1001-singlet population when the 1001-triplets are resonant with the 0110-triplets unless the levels on the outer dots are degenerate, the levels on the middle dot are degenerate, or $J = U$. This is in good accordance with the results from the master equation. If none of those conditions are fulfilled, the singlet population can be made to approach 1 for a range of parameter values. We would like to investigate the parameter space further to find an optimal parameter configuration, which maximizes the steady state population for parameters that are experimentally achievable.

The findings of this project suggest that specific multi-electron entangled states can be realized by engineering the coupling of a system to reservoirs and tuning the internal system parameters. Therefore, it would be of great interest to look into other dot networks and investigate whether they can be tuned to realize other, potentially more complicated, entangled states.

Appendix A

Quantum Mechanics

In this appendix, we briefly review a selection of concepts from quantum mechanics of closed quantum systems that we have used in thesis. Closed quantum systems are systems that do not interact with their environment. Throughout the text, we set Planck's constant $\hbar = 1$.

Unless otherwise noted, the sections are based on Ref. [3].

A.1 Pure States

The state of a system is a full description of the system. Quantum states are represented by rays in Hilbert space. For a two dimensional Hilbert space spanned by the orthogonal states $|0\rangle$ and $|1\rangle$, the state $|\psi\rangle$ is in general a superposition

$$|\psi\rangle = c_1 |0\rangle + c_2 |1\rangle \tag{A.1}$$

$$\langle\psi|\psi\rangle = 1, \quad |c_1|^2 + |c_2|^2 = 1 \tag{A.2}$$

where the last equation shows that we choose the normalized vector as representative of the ray. The coefficients c_1 and c_2 are in general complex numbers, and the phase difference between them is experimentally accessible.

A.2 Measurements

An observable is a physical property of the system which in principle could be measured. An observable is represented by a Hermitian operator

O such that $O^\dagger = O$.

The measurement of the observable collapses the state into an eigenstate of operator O. For this example, we take the states $|0\rangle$ and $|1\rangle$ in Eq. A.1 to be eigenstates of O with eigenvalues 0 and 1, respectively. The outcome of the measurement is 0 with a priori probability $|a|^2$ and 1 with probability $|b|^2$. The expectation value of the operator $\langle O \rangle$ is

$$\langle O \rangle = \langle \psi | O | \psi \rangle \tag{A.3}$$

A.3 Unitary Evolution

The time evolution of a quantum state in a closed system is described by a unitary operator $U(t - t_0)$ relating the state at t_0 to the state at t

$$|\psi(t)\rangle = U(t - t_0) |\psi(t_0)\rangle . \tag{A.4}$$

Infinitesimal time evolution is governed by the Schrödinger equation

$$i\frac{\mathrm{d}|\psi\rangle}{\mathrm{d}t} = H(t)|\psi\rangle \tag{A.5}$$

where $H(t)$ is the Hamiltonian or total energy operator of the system. If H is time independent, the time evolution operator is

$$U(t - t_0) = e^{-iH(t-t_0)}. \tag{A.6}$$

As a concrete example of a Hamiltonian, a single particle with mass m moving in a one dimensional potential $V(x)$ is described by[24]

$$H = \frac{p^2}{2m} + V \tag{A.7}$$

where p is the momentum operator. In the x-basis, the momentum operator is [24]

$$p = -i\frac{\mathrm{d}}{\mathrm{d}x}. \tag{A.8}$$

A.4 Infinite Well Potential

In Chap. 2 and Chap. 4, we use the infinite well potential to model quantum dots. In this section, we discuss it more generally. The infinite

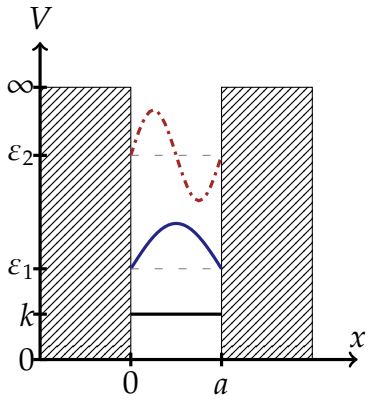

Figure A.1: One dimensional infinite well of width a and bottom at k. The ground state and first excited state ($n = 1$ and $n = 2$ in Eq. A.10) are plotted in blue and dashdotted red shifted upwards by their energy ε_n.

well potential is one of the few potentials that has an exact solution of the Schrödinger equation.[25] The infinite well potential is defined as

$$V(x) = \begin{cases} k & \text{for } 0 < x < a \\ \infty & \text{elsewhere} \end{cases} \tag{A.9}$$

where k is a constant and a is the width of the well. We plot the potential in Fig. A.1.

Solving Schrödinger's equation for this potential yields the wave function of the nth eigenstate ψ_n and the corresponding energy E_n

$$\psi_n = \sqrt{\frac{2}{a}} \sin\left(n\pi\frac{x}{a}\right) \tag{A.10}$$

$$\varepsilon_n = \frac{\pi^2 n^2}{2ma^2} + k \tag{A.11}$$

$$n = 1, 2, \ldots$$

The section is based on Ref. [24].

A.5 Perturbation Theory

In Chap. 4, we use perturbation theory to estimate the outgoing rates of states with electrons on the outer dots only due to their small coupling to states with electrons on the middle with outgoing rates from a direct coupling to the drain. In this section, we present the corrections, due to a perturbation, of the eigenstates and eigenenergies up to second order.

Perturbation theory is a method to find approximate solutions to the Schrödinger equation for potentials perturbed from a potential that leads

to exact solutions of the Schrödinger equation. We write the Hamiltonian of the perturbed problem as $H = H_0 + H'$

The first and second order corrections to the eigenstates of the unperturbed problem are

$$\left|\psi_i^1\right\rangle = \sum_{j\neq i} \frac{\left\langle\psi_j^0\right| H' \left|\psi_i^0\right\rangle}{E_i^0 - E_j^0} \left|\psi_j^0\right\rangle \tag{A.12}$$

$$\left|\psi_i^2\right\rangle = \sum_{j\neq i} \left[\sum_{k\neq i} \left[\frac{\left\langle\psi_j^0\right| H' \left|\psi_k^0\right\rangle \left\langle\psi_k^0\right| H' \left|\psi_i^0\right\rangle}{\left(E_i^0 - E_k^0\right)\left(E_i^0 - E_j^0\right)} \right] - \frac{\left\langle\psi_i^0\right| H' \left|\psi_i^0\right\rangle \left\langle\psi_j^0\right| H' \left|\psi_i^0\right\rangle}{\left(E_i^0 - E_j^0\right)^2} \right] \left|\psi_j^0\right\rangle \tag{A.13}$$

where $\left|\psi_i^n\right\rangle$ is the nth order correction, $\left|\psi_l^0\right\rangle$ is the lth eigenstate of the unperturbed problem, and E_l^0 is the energy of the l'th unperturbed eigenstate. From Eq. A.12 we see that the correction of state j is small if $\left\langle\psi_j^0\right| H' \left|\psi_i^0\right\rangle \ll E_i^0 - E_j^0$.

We use the corrections to the states in Chap. 4, but for completeness, the first and second order corrections to the energies of the unperturbed problem are

$$E_i^1 = \left\langle\psi_i^0\right| H' \left|\psi_i^0\right\rangle \tag{A.14}$$

$$E_i^2 = \sum_{j\neq i} \frac{\left|\left\langle\psi_i^0\right| H' \left|\psi_j^0\right\rangle\right|^2}{E_i^0 - E_j^0} \left|\psi_j^0\right\rangle \tag{A.15}$$

The section is based on Ref. [25].

A.6 Second Quantization

In principle, the possible states of N electrons can be written out as in Sec. 3.1.2, but it is more convenient to work in second quantization. In second quantization, we only need the occupation number of each single particle state whereas in first quantization, we have to keep track of the state of the individual electron.

We find the N-particle basis states in the following way: First we choose an ordered and complete basis of single particle states $\{|\nu_1\rangle, |\nu_2\rangle, \cdots\}$. Then we write the occupation number of all the single particle states n_i in a ket under the restriction that the total occupation number is N

$$|n_1, n_2 \cdots\rangle \tag{A.16}$$

$$\sum_i n_i = N \tag{A.17}$$

We define creation and annihilation operators for each single particle state $c_i^\dagger$ and c_i that raise or lower the occupation number of state i by one respectively. Then we may write our basis states in terms of creation operators acting on the vacuum state $|0\rangle$ as

$$|n_1, n_2 \cdots\rangle = \left(c_1^\dagger\right)^{n_1} \left(c_2^\dagger\right)^{n_2} \cdots |0\rangle\,. \tag{A.18}$$

The operator algebra of the fermionic creation and annihilation operators is

$$\{c_i^\dagger, c_j^\dagger\} = 0 \tag{A.19}$$

$$\{c_i, c_j\} = 0 \tag{A.20}$$

$$\{c_i, c_j^\dagger\} = \delta_{ij}. \tag{A.21}$$

where the anti-commutator of two operator A and B is $\{A, B\} = AB + BA$.

The antisymmetry requirement from Sec. 3.1.2 is incorporated by requiring Eq. A.19. Eq. A.20 follows by Hermitian conjugation of Eq. A.19, and Eq. A.21 follows from assuming that the value of the anti-commutator acting on the vacuum state can be taken as an operator identity. We also see that Pauli's exclusion principle is built into the formalism from Eq. A.19 by setting $i = j$.

When working with anticommuting creation and annihilation operators, it is very important to be consistent with the order of the single particle state basis and the corresponding operators. Otherwise sign errors might occur. More explicitly, it is important to note that if $|1, 1\rangle = c_1^\dagger c_2^\dagger |0\rangle$ then $c_2^\dagger c_1^\dagger |0\rangle = -|1, 1\rangle$ due to the anti-commutation relation of the creation operators in Eq. A.19.

The section until this point is based on Ref. [11]

For the calculations in Sec. 4.1.2 and Sec. 4.2, we use the triplet states from Eq. 3.13, Eq. 3.14 and Eq. 3.15 and the singlets occupying two orbitals a and b in Eq. 3.16 and one orbital in Eq. 3.17 written in second quantization.

We write the triplet states from Eq. 3.13, Eq. 3.14 and Eq. 3.15 as

$$|T_+\rangle = c_{a\uparrow}^\dagger c_{b\uparrow}^\dagger |0\rangle \tag{A.22}$$

$$|T_-\rangle = c_{a\downarrow}^\dagger c_{b\downarrow}^\dagger |0\rangle \tag{A.23}$$

$$|T_0\rangle = \frac{1}{\sqrt{2}} \left(c_{a\uparrow}^\dagger c_{b\downarrow}^\dagger + c_{a\downarrow}^\dagger c_{b\uparrow}^\dagger\right) |0\rangle\,, \tag{A.24}$$

the singlet occupying two orbitals in Eq. 3.16 as

$$|S\rangle = \frac{1}{\sqrt{2}}\left(c^{\dagger}_{a\uparrow}c^{\dagger}_{b\downarrow} - c^{\dagger}_{a\downarrow}c^{\dagger}_{b\uparrow}\right)|0\rangle\,, \tag{A.25}$$

and the singlet occupying one orbital a in Eq. 3.17 as

$$\left|\psi\right\rangle_{aa} = c^{\dagger}_{a\uparrow}c^{\dagger}_{a\downarrow}\,|0\rangle\,. \tag{A.26}$$

Appendix B

Incoming and Outgoing Rates

In this appendix, we study the influence of the incoming and outgoing rates on the steady state 1001-singlet population.

In Fig. B.1, we plot the peaks of the steady state population S_p from Fig. 4.8 as a function of the energy of the lowest orbital on the middle dot $\overline{\varepsilon_M}$ for different values of the outgoing rate $\overline{\gamma}_{out}$. We see that as $\overline{\gamma}_{out}$ increases, the maximal value of S_p decreases. This is because the width of all states with one or more electrons on the middle dot is proportional to $\overline{\gamma}_{out}$. When the width of the states is increased, it is more difficult to tune the parameters such that only the triplet states are on resonance, as discussed in Sec. 4.1.3.

In Fig. B.2, we plot the maximal value of the steady state population of the 1001-singlet state S_p from Fig. 4.8 and the 0000-state of the empty dot Z_p as a function of ingoing rate γ_{in}. We see that as the ingoing rate goes to zero, the steady state of the dot approaches the empty dot as we would expect for the situation where electrons are allowed to leave the dot network but not to enter it. For the specific parameters used to make the four subfigures in Fig. B.2, the incoming rate is as low as $\gamma_{in} \sim 0.1\gamma_{out} = 0.1t$ before the empty dot state gets a significant population in the steady state. We have not yet investigated whether this property is universal or a feature of the specific parameters.

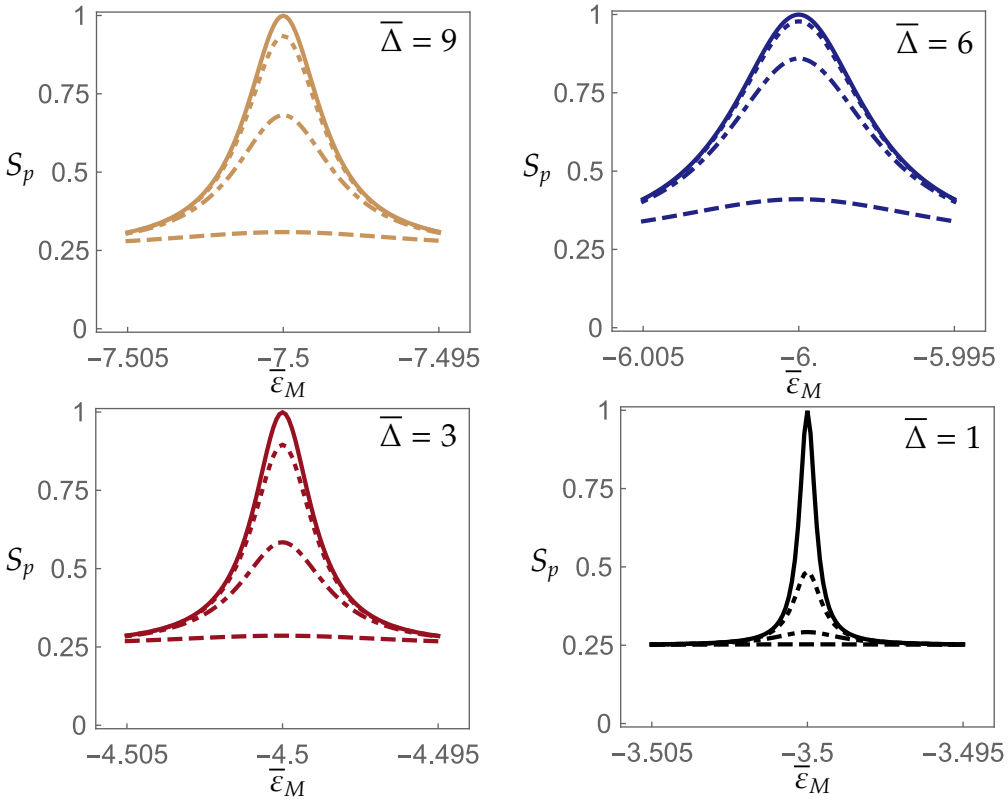

Figure B.1: Singlet population peaks for different outgoing rates. The four insets are zoom-ins on the peaks in Fig. 4.8 and show the peak in singlet population as a function of the energy of the lowest orbital on the middle dot $\overline{\varepsilon}_M$ for level spacing on the middle $\overline{\Delta} = 1, 3, 6, 9$ for different outgoing rates $\overline{\gamma}_o ut$. The full lines correspond to $\overline{\gamma}_{out} = 0.005$, the dotted lines to $\overline{\gamma}_{out} = 0.03$, the dotdashed lines to $\overline{\gamma}_{out} = 0.05$, and the dashed lines to $\overline{\gamma}_{out} = 0.1$. We varied $\overline{\varepsilon}_M$ in steps of 10^{-4}. The other parameters are $\overline{U} = 8$, $\overline{J} = 2$, and $\overline{t} = 0.005$.

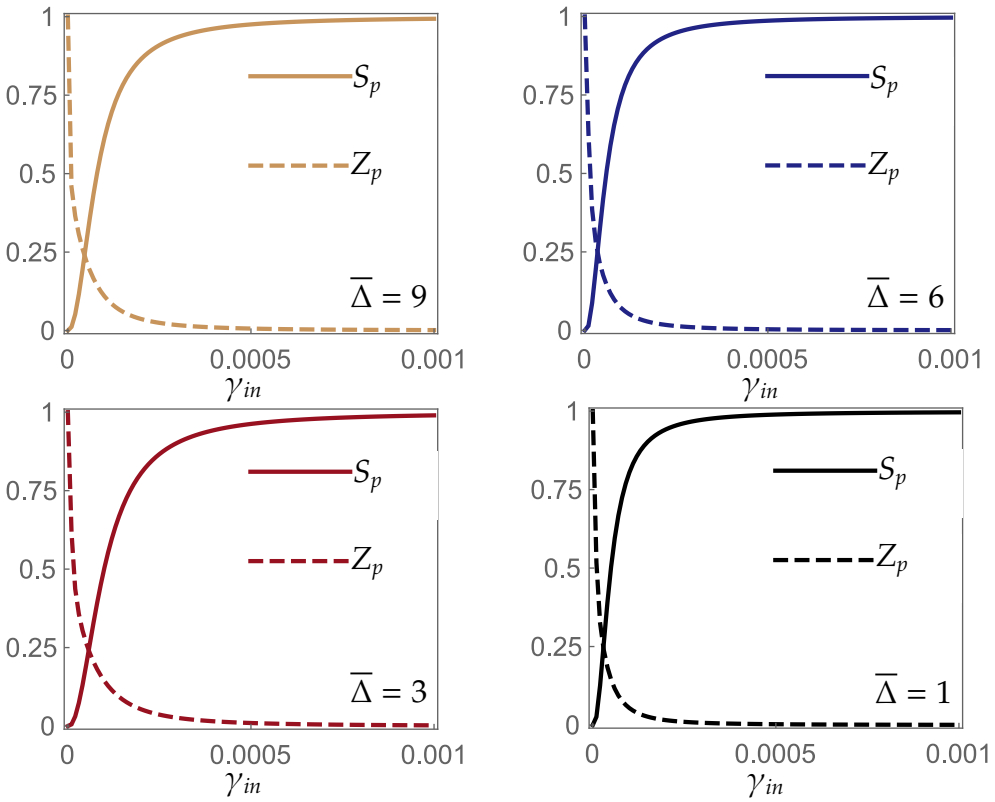

Figure B.2: Maximal singlet population and empty dot population in the steady state as a function of γ_{in}. The four insets show the maximal singlet population and the empty dot population in the steady state as functions of the incoming rate γ_{in}. The full lines are the singlet population S_p, and the dashed lines are the population of the empty state Z_p. As we would expect, the population of the empty state goes to 1 as the incoming rate goes to zero. For these four parameter configurations, we see that the steady state population of the empty state becomes significantly different from zero for $\gamma_{in} \sim 0.1\gamma_{out}$. We varied γ_{in} in steps of $5 \cdot 10^{-5}$. The other parameters are $U = 8$, $J = 2$, $\gamma_{out} = t = 0.005$.

APPENDIX C

Exchange Integral

In this appendix, we study the influence of the exchange intergral[26] $\bar{J}$ relative to $\overline{U}$, defined in Eq. 4.16 on the steady state 1001-singlet population S_p. As in the main text, a bar indicates that the parameter is relative to the incoming rate γ_{in}.

In Fig. C.1 on the next page, we plot S_p as a function of the energy of the lowest orbital on the middle dot ε_M for different values of the exchange integral $\bar{J}$ for $\overline{U} = 8$. We see that, except for the top and bottom panel, varying $\bar{J}$ preserves the peak height whereas the position changes. The peak position is given by

$$\bar{\varepsilon}_M = \frac{1}{2}(\bar{J} - \overline{U} - \overline{\Delta}), \tag{C.1}$$

where $\overline{\Delta}$ is the level spacing on the middle dot. The equation follows from the requirement that the 0110-triplet states are resonant with the 1001-triplets or $E_{0110T} = 0$, see Eq. 4.24. In the top panel, there is no peak even though we expect to see one at $\bar{\varepsilon}_M = -5.5$ from Eq. C.1. It is because for $\bar{J} = 0$, the 0110-triplet and 0110-singlet states are degenerate. The blockade phenomenon, described in Sec. 4.1.3, that should lead to an increase in singlet population utilizes the energy difference between the two, and therefore it is not present for degenerate 0110-singlet and 0110-triplets. In the bottom panel where $\bar{J} = \overline{U}$, there is no peak even though we expect to find one at $\bar{\varepsilon}_M = -1.5$ from Eq. C.1. This is due to the interference effect described in Sec. 4.2.5

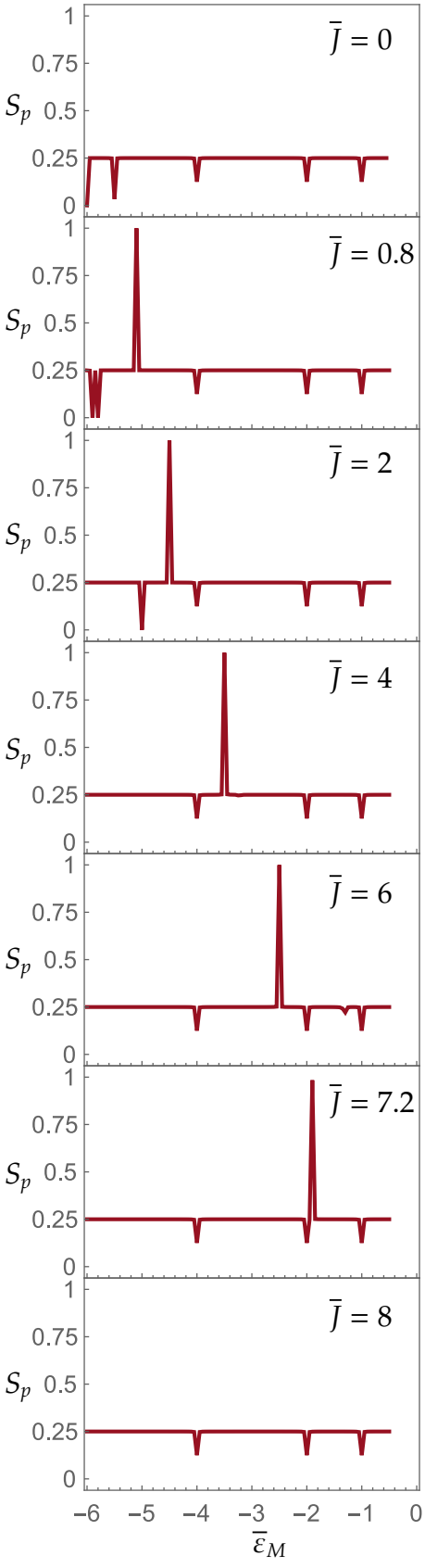

Figure C.1: Steady state population of the 1001-singlet as a function of the energy of the lowest level on the middle dot $\overline{\varepsilon}_M$ for detuning on the middle dot $\overline{\Delta} = 3$ for different values of $\overline{J}$. The position of the peaks in the middle panels can be understood by Eq. C.1. The absence of peaks in the top and bottom panel can be understood from the degeneracy of the 0110-singlet and 0110-triplet states for $\overline{J} = 0$ and from the interference described in Sec. 4.1.3 for $\overline{J} = \overline{U}$. The dips in the singlet populations are due to other resonances, see Sec. 4.3.The other parameters are $\overline{U} = 8$, $\overline{\varepsilon}_R = -\overline{\varepsilon}_L = 1$, and $\overline{\gamma}_{out} = \overline{t} = 0.005$. We vary $\overline{\varepsilon}_M$ in steps of 0.05.

Bibliography

[1] R.P. Muller and R. Blume-Kohout. The Promise of Quantum Simulation. *ACS Nano*, 2015.

[2] D. P. DiVincenzo. The Physical Implementation of Quantum Computation. *Prepared for Fortschritte der Physik special issue, Experimental Proposals for Quantum Computation*, 2000.

[3] J. Preskill. Lecture notes for ph219/cs219: Quantum information. Accesible via http://www.theory.caltech.edu/people/preskill/ph229/, 1997-2015.

[4] R. P. Feynman. Simulating Physics with Computers . *Int. J. Theor. Phys.*, 1982.

[5] I.M. Georgescu et al. Quantum Simulation. *Rev. Mod. Phys.*, 2014.

[6] T.D. Ladd et al. Quantum Computers. *Nature*, 2010.

[7] D. Loss and D. DiVincenzo. Quantum Computation with Quantum Dots. *Phys. Rev. A*, 1998.

[8] R. Vrijen et al. Electron-spin-resonance Transistors for Quantum Computing in Silicon-germanium Heterostructures. *Phys. Rev. A*, 2000.

[9] F. H. L. Koppens et al. Driven Coherent Oscillations of a Single Electron Spin in a Quantum Dot. *Nature*, 2006.

[10] R. Hanson. Spins in Few-Electron Quantum Dots. *Rev. Mod. Phys.*, 2007.

[11] H. Bruus and K. Flensberg. *Many-Body Quantum Theory in Condensed Matter Physics*. Oxford University Press, Inc., 2004.

[12] D. M. Zumbühl. *Coherence and Spin in GaAs Quantum Dots*. PhD thesis, Harvard University, 2004.

[13] J. K. Perron et al. A new Regime of Pauli-Spin Blockade. *ACS Nano*, 2015.

[14] L.P. Kouwenhoven et al. Few-electron Quantum Dots. *Rep. Prog. Phys.*, 2001.

[15] K. Ono et al. Current Rectification by Pauli Exclusion in a Weakly Coupled Double Quantum Dot System. *Science*, 2002.

[16] Y. C. Sun et al. Spin Blockade with Spin Singlet Electrons . *Appl. Phys. Lett.*, 2012.

[17] G. Grynberg C. Cohen-Tannoudji, J. Dupont-Roc. *Atom-Photon Interactions*. Wiley-VCH, 2004.

[18] P. Meystre and M. Sargent. *Elements of Quantum Optics, 4th edition*. Springer, 2007.

[19] Master equation. https://quantiki.org/wiki/master-equation.

[20] C.A. Brasil et al. A Simple Derivation of the Lindblad Equation. *Revista Brasileira de Ensino de Fisica*, 2013.

[21] L. Gaudreau et al. Coherent control of three-spin states in a triple quantum dot. *Nature Physics*, 2012.

[22] J. Medford et al. Quantum-Dot-Based Resonant Exchange Qubit. *Phys. Rev. Lett.*, 2013.

[23] K. Eng et al. Isotopically Enhanced Triple-quantum-dot Qubit. *Sci. Adv.*, 2015.

[24] D. J. Griffiths. *Introduction to Quantum Mechanics*. Pearson Education, Inc., 2005.

[25] J.J. Sakurai and J. J. Napolitano. *Modern Quantum Mechanics Second Edition*. Pearson Education Limited, 2014.

[26] Stephen Blundell. *Magnetism in Condensed Matter*. Oxford University Press, Inc., 2001.